https://ntrs.nasa.gov/search.jsp?R=19940021648 2020-06-16T14:10:33+00:00Z

IN-05
208973
40 p

NASA Technical Memorandum 103988

Design Optimization of High-Speed Proprotor Aircraft

David R. Schleicher, James D. Phillips, and Kevin B. Carbajal

(NASA-TM-103988) DESIGN OPTIMIZATION OF HIGH-SPEED PROPROTOR AIRCRAFT (NASA) 40 p

N94-26151

Unclas

G3/05 0208973

April 1993

National Aeronautics and Space Administration

NASA Technical Memorandum 103988

Design Optimization of High-Speed Proprotor Aircraft

David R. Schleicher, James D. Phillips, and Kevin B. Carbajal
Ames Research Center, Moffett Field, California

April 1993

National Aeronautics and
Space Administration

Ames Research Center
Moffett Field, California 94035-1000

Contents

PAGE ii INTENTIONALLY BLANK

PRECEDING PAGE BLANK NOT FILMED

Summary

NASA's high-speed rotorcraft (HSRC) studies have the objective of investigating technology for vehicles that have both low downwash velocities and forward flight speed capability of up to 450 knots. This paper investigates a tiltrotor, a tiltwing, and a folding tiltrotor designed for a civil transport mission. Baseline aircraft models using current technology are developed for each configuration using a vertical/short takeoff and landing (V/STOL) aircraft design synthesis computer program to generate converged vehicle designs. Sensitivity studies and numerical optimization are used to illustrate each configuration's key design tradeoffs and constraints. Minimization of the gross takeoff weight is used as the optimization objective function. Several advanced technologies are chosen, and their relative impact on future configurational development is discussed. Finally, the impact of maximum cruise speed on vehicle figures of merit (gross weight, productivity, and direct operating cost) is analyzed.

The three most important conclusions from the study are: (1) payload ratios for these aircraft will be commensurate with current fixed-wing commuter aircraft, (2) future tiltrotors and tiltwings will be significantly lighter, more productive, and cheaper than competing folding tiltrotors, and (3) the most promising technologies are an advanced-technology proprotor for both the tiltrotor and the tiltwing and advanced structural materials for the folding tiltrotor.

Nomenclature

C_D	drag coefficient based on wing area
C_L	vehicle lift coefficient
C_T	rotor thrust coefficient
C_P	rotor power coefficient
c/D	wing chord-to-propeller diameter ratio
L/D	vehicle lift-to-drag ratio
M	Mach number
M_{cruise}	cruise Mach number
M_{DD}	drag divergence Mach number
$M_{H.75R}$	helical Mach number at 75% rotor radius
OEI	one engine inoperative
rpm	revolutions per minute
sfc	specific fuel consumption
σ	rotor solidity
TAS	true airspeed
t/c	thickness-to-chord ratio
y_{eng}	engine spanwise distance

1. Introduction

Figure 1 illustrates the historical trend of disk loading versus cruise speed for vertical takeoff and landing (VTOL) aircraft. The low disk loading aircraft, such as helicopters and tiltrotors, have the advantage of efficient hover and low downwash velocities but tend to have low cruise speeds. The high disk loading aircraft, such as tiltwings and ducted fans, have higher cruise speeds but poor hover efficiency and higher downwash velocities.

The goal of NASA's high-speed rotorcraft (HSRC) investigations is to develop technology for an aircraft that combines low downwash characteristics with high cruise speed. For the purposes of this study, a disk loading limit of 21 lb/ft^2 was chosen to keep proprotor downwash velocities low enough to allow ground personnel to approach the aircraft from any direction without being overturned (see ref. 24). A high, 450-knot cruise speed was chosen to push the vehicles to the limits of past propeller-powered aircraft.

To help guide its future research, NASA sponsored four helicopter manufacturers (Bell, Boeing, McDonnell-Douglas, and Sikorsky) to perform studies to both determine the most effective vehicles to fulfill the HSRC requirements and to provide recommendations of enabling technologies necessary to develop these vehicles (refs. 1–4). The consensus resulting from these studies is that the most effective vehicles for attaining high-speed cruise and a benign downwash environment are aircraft that utilize tilting proprotors as their means of propulsion (e.g., tiltrotors and tiltwings).

This paper compares three high-speed candidate vehicles: a tiltrotor, a tiltwing, and a folding tiltrotor. The paper is organized into eleven sections. Following this introduction, the three configurations and the proposed mission are described. The third section explains how the design synthesis code sizes the candidate configurations. Next, the assumptions made for each of the current-technology vehicles are provided. The fifth section discusses the ground rules followed in the optimization process. Then, the sixth section discusses the optimized current-technology configuration results. The seventh section identifies a number of proposed advanced technologies and examines their respective effects on vehicle design and gross weight. The results of combining the advanced-technology assumptions and re-optimizing the three vehicle configurations are presented in the eighth section.

Next, the effects of increasing the disk loading limit on vehicle gross weight are investigated. The tenth section addresses the impact of cruise speed on the optimization of the advanced vehicles with respect to three figures of merit: gross weight, productivity, and direct operating cost. Finally, results and observations from the overall study are summarized.

2. Configurations and Mission

The three proprotor-driven aircraft configurations selected for this study are shown in figure 2. All three vehicles use their proprotors for lift during a vertical takeoff or landing; they tilt their proprotors over to achieve wing-borne flight. The manner in which each achieves conversion from vertical to high-speed forward flight constitutes the major difference between the three configurations. Furthermore, these different conversion methods result in distinct advantages and disadvantages to each of the three aircraft.

The tiltrotor is a derivative of three prior lower speed, lower disk loading tiltrotor aircraft: XV-3, XV-15, and V-22. Conversion to forward flight is accomplished by tilting its two wingtip-mounted proprotors from vertical, through a 90° angle, to a forward-facing position for cruise. This process results in a continuous change in the share of lift borne by the rotor and the wing. Due to its nontilting wing, the conversion behavior of tiltrotors typically provides insensitive conversion characteristics, but the vehicle's proprotor downwash generates a significant download on the wing in hover.

The tiltwing being studied is an advanced derivative of four earlier medium-speed, medium disk loading tiltwing aircraft: VZ-2, X-18, XC-142, and CL-84. Unlike the tiltrotor, a tiltwing rotates its wing together with the proprotor during conversion from hover to forward flight. This method of conversion eliminates the significant download on the wings of tiltrotors, but new problems are introduced, including more sensitive conversion characteristics and the possibility of wing stall during steep descents.

Yet to be flight-tested, the folding tiltrotor configuration hovers and converts like the tiltrotor except that once fully converted and full wing lift has been achieved in airplane-mode flight, the proprotor is then stopped and indexed, and the blades are folded back along the wingtip nacelles. In order to enable the proprotor to be declutched from the engine, thrust in this flight mode must be provided by a separate thrusting device, such as a turbofan engine. By stowing the proprotor, the folding tiltrotor avoids the high drag and wing-proprotor instability of high-speed forward flight faced by the tiltrotor and tiltwing, but the folding tiltrotor encounters its own disadvantages. The biggest disadvantages are: (1) the necessity of a convertible engine, which is heavier and less fuel efficient than an equivalent turboshaft engine, (2) the additional weight and complexity of a blade-folding mechanism, and (3) the additional drag caused by the stowed proprotor in high-speed flight.

For the purposes of this paper, each of the three advanced VTOL concepts were evaluated for a single civil transport mission. The baseline mission required the aircraft to carry 30 passengers (6000 lb) for a range of 600 n. mi. Shown in figure 3, the civil transport mission is based on a candidate mission used in the HSRC studies (refs. 1–4). The baseline mission begins with a 1-minute hover and takeoff at sea level on a hot day (standard day + 15°C). The vehicle then converts to its cruise configuration along a 6° ascending and accelerating flight path, still during the assumed hot day. Next, a climb at maximum rate of climb is performed until the specified cruise altitude is reached. At the fixed altitude, the vehicle cruises at 450 knots TAS until its 600-n. mi. range is completed (with range credit for previous conversion and climb segments). Having flown its 600-n.mi. range, the vehicle descends to low altitude (with no fuel credit) and conversion-mode speed and then performs a decelerating conversion along a 6° descending glide path. Finally, the vehicle hovers for 1 minute at sea level on a hot day, and then lands with 10% mission fuel reserve.

In addition to the basic mission profile, the following assumptions were made: to accomplish an out-of-ground-effect hover with one engine inoperative, the engines were sized with a power rating 25% higher than the maximum all-engines-operating takeoff rating; conversion follows a 6° ascending, 0.2-g accelerating glide slope; the 0.2-g acceleration was a typical value from ongoing tiltwing simulations (ref. 5); reconversion is limited to a 6° descending, 0.04-g decelerating glide path. Moreover, certain mission-related equipment weights were fixed:

1. Fixed equipment weight = 4000 lb
2. Avionics weight = 800 lb
3. Operating items (including crew, attendant, miscellaneous crew and passenger service items, engine oil, and trapped fuel) = 775 lb.

3. Aircraft Synthesis

In order to size the three candidate rotorcraft as well as to study the effects of various design parameters on them, a multidisciplinary design synthesis computer program was used. The sizing of all aircraft in this study was conducted using the Ames version of VASCOMP II (V/STOL

Aircraft Sizing and Performance Computer Program) (ref. 6). The Ames version has been extensively modified and updated for use in studying a wide spectrum of V/STOL concepts.

More specifically, the current investigation of HSRC vehicles has required the modification of the original VASCOMP II for optimizing vehicles for high-speed proprotor-borne flight. Significant changes to VASCOMP II include the following: (1) the addition of a numerical parameter optimizer around the original design convergence methodology, (2) development of a mission module to simulate tiltrotor and tiltwing conversions and reconversions, (3) incorporation of a wing-weight estimation method that includes aeroelastic stiffness requirements and wing sweep, (4) inclusion of a simple method to analyze proprotor performance in high-speed axial flight, (5) modifications to allow for the use of convertible engines in shaft or thrust mode during any mission segment, (6) addition of an enhanced drag divergence prediction method, and (7) development of a simple method to predict wing-body and wing-nacelle interference drag. These changes are discussed later in this paper.

VASCOMP is structured as shown in figure 4. After a brief overview of the VASCOMP aircraft-sizing process, the method by which the design code models a vehicle's aerodynamics, propulsion, weights, and mission performance will be discussed. Finally, details of the numerical optimizer used will be addressed.

3.1 Aircraft Sizing

VASCOMP requires a list of parameters that define the geometry, aerodynamics, propulsion performance, and weight trends for the vehicle in question. These inputs, combined with a definition of the vehicle's mission and an initial guess at the gross weight of the vehicle, are then used by VASCOMP to determine the vehicle's detailed geometry and weight breakdown. The weight available for fuel is determined by subtracting the sum of the vehicle component weights from the gross weight estimate. VASCOMP then performs a mission simulation on the now-defined vehicle. For each individual mission segment, the amount of fuel required for the vehicle to fly at the prescribed conditions is calculated. The successive segment fuel weights are summed to determine the weight of fuel required for the total mission.

VASCOMP then compares the weight of the fuel available and the weight of the fuel required. If the former is greater than the latter, the vehicle is oversized for the given mission, so the gross weight estimate is decreased and the sizing loop is repeated. However, if fuel available is less than fuel required, the vehicle's mission requires more fuel than available onboard, and thus the vehicle is undersized. The gross weight estimate is increased, and the sizing loop is repeated. The secant method is used to rapidly match the fuel available to the fuel required to within a specified tolerance. Detailed information, including vehicle dimensions, engine power, drive system torque, parasite drag breakdown, mission segment time history, etc., are provided as output to the user.

3.2 Aerodynamics

Airframe aerodynamics are based on a component drag buildup. The parasite drag of each vehicle component is calculated from the combination of its wetted area, a skin friction coefficient with Reynolds number correction, and a profile drag factor that takes into account two- and three-dimensional aerodynamic effects. Induced drag is determined as a function of wing lift coefficient, wing aspect ratio, and span (Oswald) efficiency factor, the latter calculated according to the method in reference 7. Wing compressibility drag effects are modeled first by determining the drag divergence Mach number (M_{DD}) using the method described in reference 8, and second, by calculating a ΔC_D that is cubic with respect to the difference between M_{cruise} and M_{DD}.

Wing-fuselage and wing-nacelle interference drag are estimated based on interference work reported in references 9–11. Additional drag due to antennae, lights, flap gaps, etc., is split into two categories: a fixed increase in flat-plate drag area and an incremental C_D that is scaled with wing area.

3.3 Propulsion

3.3.1 Proprotor performance estimation– Proprotor performance estimation is based on a combination of an empirically derived hover performance map with an analytical cruise performance method. An experimentally based input table of proprotor figure of merit vs. C_T/σ and blade-tip Mach number define the proprotor hover performance. The level of hover performance assumed was based on V-22 test data (ref. 12) and high blade-tip Mach number performance based on rotor experiments (ref. 13). The analytical cruise performance method is detailed in reference 14. This method defines C_P as the sum of profile, induced, and parasite power. These calculated powers are a relatively simple function of advance ratio, C_T, solidity, and average profile power coefficient. Compressibility is modeled as a quartic function of the difference between the helical tip Mach number at 3/4 rotor radius ($M_{H.75R}$) and the rotor airfoil M_{DD}.

3.3.2 General engine sizing– Engines are sized for the most critical of three conditions: hover, conversion, or cruise. Engine and nacelle dimensions and weight were modeled as linear functions of the square root of the maximum engine power.

3.3.3 Tiltrotor/tiltwing engine sizing– The tiltrotor and tiltwing designs require the use of a turboshaft engine. For these configurations, the General Electric GLC38-T1M1 turboshaft engine, a derivative of the GE27 Modern Technology Demonstrator Engine (MTDE), was used.

To generate the data required for VASCOMP to model and scale the engine, tables of airflow, fuel flow, gas generator speed, and power as a function of altitude, Mach number, and power setting were generated using a General Electric GLC38-T1M1 engine model. Using the corrected-parameter method (refs. 15 and 16), these data were reduced to a nondimensional form with the engine performance parameters being functions of corrected aircraft speed (Mach number) and corrected turbine inlet temperature (power setting). The corresponding values of corrected shaft power, corrected fuel flow, corrected generator speed, and corrected airflow determined in this manner are then used as the input engine data for VASCOMP.

Also included in VASCOMP is the ability to specify limits on engine fuel flow, turbine speed, gas generator speed, and maximum torque. Values for these parameters were also available from the engine model.

Because these configurations may require that their proprotors operate at a lower rpm in cruise, engine off-design performance needed to be modeled. This was done using a quadratic dropoff in power at nonoptimum turbine speeds.

3.3.4 Folding tiltrotor engine sizing– Since the folding tiltrotor requires shaft power for hover and conversion and fan thrust for cruise operation, a convertible engine is required. A study performed for NASA Lewis Research Center to define and compare convertible engine concepts for high-speed rotorcraft (ref. 17) concluded that a convertible engine using variable-inlet guide vanes (VIGV) would be well suited to this type of vehicle. The VIGV fan engine was judged to be the simplest of the concepts examined, would be the least expensive to develop, and offers good shaft/thrust power sharing while operating between the shaft power and thrust modes. In addition, previous demonstrations of this concept using a TF-34 engine were performed at NASA Lewis during the Convertible Engine Systems Technology (CEST) test program.

The GE38/CE4 concept engine (ref. 18) was chosen as a model for the powerplant of the folding tiltrotor. This engine uses a mixed exhaust flow with partial variable-inlet and -exit guide vanes and is based on a growth version of the current-technology GLC38 core. The input tables for this engine contained data similar to those for the turboshaft engine with the addition of three tables that contained the corrected thrust, thrust-mode-corrected fuel flow, and thrust-mode-corrected gas generator speed as functions of Mach number and corrected turbine inlet temperature.

3.4 Weights

Component weights are determined from detailed statistical weight equations. A technology factor scales the calculated weight to specify a particular level of advanced technology.

Wing weight deserves special attention. For proprotor-driven flight, wing weight may be sized by whirl flutter or a 2-g jump takeoff condition instead of bending moments during cruise. To take this into account, VASCOMP's wing-weight prediction methodology was modified to determine the wing weight based on jump takeoff loads and whirl flutter avoidance. The algorithm used was based on a method developed to model tiltrotor wings (ref. 19). The weight of additional wing span beyond that of the proprotor hub, necessary for tiltwings, was calculated using cruise bending moment criteria.

3.5 Mission Definition

VASCOMP models a given mission as a series of mission segments that are analyzed within their discrete subroutines. Mission segment options include hover/takeoff/landing, convert/reconvert, climb, descend, transfer of altitude, loiter, and cruise. For each segment, inputs (e.g., ambient temperature, power setting, glide slope) specify the particular maneuver conditions desired, and VASCOMP calculates detailed information about the steady-state maneuver (e.g., fuel required, C_L, C_D, thrust and power required) at specified time, range, or velocity steps.

3.6 Numerical Optimization

By itself, VASCOMP functions as a synthesis program that converges on a vehicle's gross weight for a given set of input parameters. However, in combination with a numerical optimizer developed at Ames, VASCOMP can be used to optimize a specified objective function with respect to any number of input parameters and constraints.

The numerical optimization method is based on the conjugate direction method of Fletcher and Reeves (ref. 20). This method uses gradient information from

sequential searches to determine the direction to the minimum of an approximate quadratic surface. The golden-section method is used for the required one-dimensional searches.

Constraints are handled with a modified exterior penalty function. The exterior penalty function is shifted into the design space by an amount set by the user. This allows the optimizer to converge at an active constraint without having excessive penalty-function curvature.

In the standard sequential unconstrained minimization, the magnitude of the penalty function has to approach infinity if a constraint is active. This makes the curvature of the penalty function also infinite near the solution, and the conjugate direction method can fail to find the correct search direction.

By shifting the edge of the penalty function past the desired boundary into the design space, the necessity for the penalty function to approach infinity in the limit is avoided. The penalty function then has less curvature, which eases the job of the unconstrained numerical method.

4. Assumptions

The goal of this study was to determine the overall effect of the differences of the three concepts on their respective gross weights.

To ensure a valid comparison, a common set of input parameters that describe the sizing, aerodynamics, and weight trends for the various components that make up the vehicle model (e.g., fuselage, wing, proprotor) was specified. These parameters were based on performance of typical turboprop transport and Bell/Boeing's CTR-22C tiltrotor, a civil derivative of the V-22 designed for 39 passengers and a 600-n. mi. mission (ref. 21).

The assumptions made in generating a baseline model will be discussed for each major component of the tiltrotor concept. In turn, each component will be examined to find out how its general sizing, performance (aerodynamic or propulsive), and weight trends were determined. Then the assumed differences for the tiltwing and folding tiltrotor models will be specified.

4.1 Tiltrotor

4.1.1 Fuselage– The fuselage is pressurized and designed to carry 30 economy-class passengers, three abreast, with one flight attendant and a cockpit crew of two. These specifications generate the fuselage length, width, and wetted area as calculated in VASCOMP. Additional parasite drag due to landing-gear fairings was based on C-141A aerodynamic performance (ref. 22). The structural weight of the fuselage was estimated using VASCOMP's internal weight-trend equation with an assumed maximum structural design equivalent airspeed of 400 knots.

4.1.2 Wing– The tiltrotor's graphite-epoxy wing is modeled after the wing design of the CTR-22C. Like the tiltrotor wings designed before it, the cantilevered wing is untapered. Wing span is determined by proprotor-fuselage clearance and proprotor size. The values of wing loading, sweep, and t/c were design parameters for optimization. A high-wing configuration was chosen for nacelle-ground clearance.

Wing aerodynamics is one of the most important performance parameters in this study. Since this study pushes the high-speed envelope of proprotor aircraft, special attention must be paid to how the high-speed aerodynamics are modeled. This study assumes typical supercritical airfoil performance—an increase of 0.05 M_{DD} over conventional airfoils. Conventional airfoil M_{DD} performance is modeled by the method in reference 8.

For low-speed flight, the baseline tiltrotor utilizes full-span, 0.25-chord, single-slotted flaps and flaperons similar to those of the V-22. The baseline airfoil and flap low-speed aerodynamic characteristics are based on those of the V-22 (ref. 12). Additional drag of flap slat, aileron gaps, and wing fasteners was taken into account by adding a ΔC_D of 0.0005.

Extra wing weight to prevent whirl flutter instability was based on required wing torsional, beam, and chord natural frequency ratios. A detailed discussion of the natural frequency ratios can be found in reference 23. From this reference, the "high-speed criterion" of 0.53, 1.04, and 1.23 for the respectively beam, chord, and torsional natural frequency ratio stiffness requirements was used in aeroelastically tailoring the tiltrotor wing for 400 knots. For speeds below and above 400 knots, these values were adjusted by a factor developed at Ames.

4.1.3 Proprotor, hub, and drive system– The general proprotor design is based on the V-22/CTR-22C rotor. One major difference is the lower design C_T/σ of 0.125 (V-22 $C_T/\sigma = 0.134$), chosen in reference 23 for the 400-knot tiltrotor. This results in a heavier proprotor weight, but allows for better maneuvering in low-speed flight.

Proprotor size was determined by disk loading and vehicle gross weight. A preliminary disk loading was chosen to be 21 lb/ft^2. Since excessive downwash velocities may be a hazard in various operational or environmental situations, one objective of NASA's HSRC studies was to define

where a practical disk loading limit would be. In their final reports, the four contractors came up with various downwash limits of between 15 and 50 lb/ft^2 (refs. 1–4). The 21-lb/ft^2 disk loading limit chosen above is a personnel-overturning moment limit for a side-by-side rotor configuration at 0° radius (ref. 24). Sufficient proprotor clearance from the fuselage was obtained by a 9-inch clearance for each proprotor.

Blade number was increased from the three-bladed configuration of the XV-15 and V-22 to a four-bladed configuration. Holding proprotor solidity constant, the addition of an extra blade increases hub weight and its associated proprotor controls but provides a potential reduction in the vehicle's sound pressure level (refs. 21 and 24).

Hover and cruise tip speeds were design parameters for optimization. Proprotor tip speed during climb was chosen as halfway between the determined hover and cruise tip speeds.

Aerodynamic performance of low disk loading proprotors is a very critical parameter in the cruise and hover performance of tiltrotor aircraft. High-speed proprotor performance is dependent on cruise speed, C_T, and compressibility drag characteristics. For the current-technology proprotor, typical cruise efficiencies of roughly 0.7 were assumed. These are similar to current-technology proprotor cruise efficiencies predicted by the four helicopter manufacturers in the High-Speed Rotorcraft Study (ref. 25).

Finally, the proprotor, hub, and drive system weights were estimated using statistical weight trends detailed in HESCOMP (ref. 26).

4.1.4 Empennage– Like the CTR-22C, the tiltrotor empennage is a conventional vertical and horizontal tail arrangement. In the pitch axis, the two major contributors of moment are the fuselage and wing. Since the fuselage size was fixed but the wing size was variable, horizontal tail area was determined by choosing an area halfway between fixed area and fixed horizontal tail volume. Since the largest generator of yaw moment, the fuselage, was fixed in size for the study, vertical tail area was fixed at 82 ft^2. Fixed area for both tail surfaces was determined by scaling down the CTR-22C tails to account for the smaller fuselage in this study. Downscaling was done using the tail volume correlations in reference 27. Horizontal tail t/c and aspect ratios were fixed at 0.12 and 4.0. Vertical tail t/c and aspect ratios were fixed at 0.12 and 2.0. VASCOMP weight-regression equations were used to predict the tail weights.

4.1.5 Flight controls– Flight control weights are determined through the statistical weight-regression equations developed in VASCOMP.

4.1.6 Miscellaneous– Drag due to antennae, air conditioning, anti-icing, and other miscellaneous items was taken to be 0.6 ft^2.

4.2 Tiltwing

Much of the analytical methodology and technical assumptions of the tiltrotor are the same for the tiltwing. This section will describe only the differences between the tiltwing and tiltrotor models.

4.2.1 Reconversion– In contrast with tiltrotors, tiltwings are limited during reconversion by wing stall. Avoiding wing stall establishes a lower bound on the ratio of wing chord to propeller diameter, as will be explained. The implication for a tiltwing with a disk loading limited to 21 lb/ft^2 is that either the wing area or the wing aspect ratio will be excessive. If the wing area is excessive, the tiltwing will have poor L/D in high-speed cruise (ref. 28). If the aspect ratio is excessive, the wing weight to prevent whirl flutter at high speed will be very high.

Historically, the chord-to-diameter ratio of tiltwing aircraft was limited to about 0.4 to prevent wing stall. For this study, instead of using chord-to-diameter limits directly, the wing-propeller aerodynamics are modeled and the chord-to-diameter ratio is varied to prevent stall during a required reconversion. This allows the effects of auxiliary drag devices and improved wing devices on wing stall to be examined more directly. The connection between wing-propeller aerodynamics and chord-to-diameter ratio is described below.

When the wing angle relative to the flight path is greater than stall angle of attack, stall is delayed in the portion of the wing immersed in the propeller wake. At sufficiently high thrust settings, the propeller turns the flow so that the local angle of attack at the wing is less than the stall angle of attack. However, if the required trim thrust is too low, the propeller-induced angle at the wing will be low and the wing will stall.

During reconversion involving decelerating and descending flight, the reduced proprotor thrust results in an increase of the local angle of attack. Additional parasite drag increases the required thrust and therefore reduces the local angle of attack during reconversion. Deploying efficient flaps further decreases the local angle of attack for two reasons. The first reason is that turning of the prop wake by the wing flaps destroys propwash momentum in the flight-path direction, creating momentum drag very much like the induced drag

of a low-aspect-ratio wing. This momentum drag must be compensated for by increased propeller thrust. The second reason is that the increased lift acting at the wing reduces the required lift component at the propeller. The propeller and wing can then be operated at a lower incidence to the flight path for a given speed; this reduces the local angle of attack at the wing directly.

Efficient turning of the prop wake by the wing requires that the wing chord with flaps deployed be comparable in size to the propeller diameter. If the wing chord is too small relative to the propeller, then the prop wake largely escapes the influence of the wing, and the beneficial momentum drag is not created. The thrust must then be reduced to keep the aircraft from accelerating along the flight path. Unfortunately, the reduction in thrust may cause wing stall.

It follows that auxiliary drag devices, more effective flaps, and wing leading-edge devices that delay stall to greater angles of attack will allow the chord-to-diameter ratio to be decreased. With this in mind, the following assumptions are made for the current-technology tiltwing. First, the wing uses double-slotted flaps with an increase in maximum lift over the basic airfoil as high as 2.0 (it is a function of thickness). Second, the stall angle of attack of the portion of wing in the prop wake (including three-dimensional effects) is 22°. Finally, the aircraft has an auxiliary drag device that creates parasite drag equivalent to 10% of the wing area. This corresponds to an increase in drag coefficient of 0.1.

To avoid the added complexity, weight, and drag of a tail rotor for pitch control in hover/conversion flight, a geared flap-control system (ref. 29) was used. This control system is assumed to provide adequate hover/conversion pitch control for a negligible increase in weight without the use of a supplemental pitch-control device.

4.2.2 Geometry– The wing span is determined by a combination of sufficient proprotor tip clearance, proprotor size, and wing extension beyond the proprotor hub. The wing extension is needed to turn the prop wake outboard of the proprotor hub for reasons explained in section 4.2.1. Since the proprotor wake contracts very rapidly and is nearly fully contracted by the time it reaches the wing, the wing does not need to extend all the way out to the proprotor tip. For this study, the wing tip distance from the center of the proprotor is fixed at 70.7% of the proprotor radius (the dimension of the fully contracted wake).

Tiltwings have a structural advantage over tiltrotors with regard to jump takeoff. The spar depth for jump-takeoff bending loads is determined largely by the wing chord, not the thickness of the wing. It is therefore not obvious whether the engines should be coincident with the proprotor. For this study, the engine position was allowed to vary with no drag penalty to examine the effect of engine position on bending relief.

4.2.3 Weights– For tiltwings, the proprotor and drive weights are computed using VASCOMP weight trends instead of the HESCOMP weight trends used for the tiltrotor. The VASCOMP weight trends are based on many propeller-driven VTOL aircraft, including previous tiltwing research aircraft. The HESCOMP weight trends are based strictly on rotors.

At the relatively low disk loading and medium vehicle size of this study, the tiltwing propeller diameters are 30 ft and larger. The largest propeller built to date is approximately 20 ft in diameter. It is unlikely that the proposed 30-ft-diameter propellers can be made stiff enough not to flap excessively through a tiltwing conversion. Therefore, the large tiltwing propellers may end up being stiff-in-plane hingeless or bearingless rotors with a consequent weight increase over conventional propellers. The VASCOMP weight trends are appropriate for estimating the weight of large proprotors since they are based on both rotors and propellers.

The tiltwing drive weight is estimated using the VASCOMP weight trends, not the HESCOMP weight trends. The justification is the same as for the proprotors. The VASCOMP data base includes many VTOL research aircraft as well as helicopters.

The tiltwing wing weight is penalized according to the VASCOMP guidelines for a double-slotted flap with track and simple hinge. This amounts to a 25% increase in weight over that of a wing with a simple flap.

4.3 Folding Tiltrotor

The folding tiltrotor uses analytical methodology and technology assumptions similar to those previously described for the tiltrotor. This section addresses the changes that were required to enable the folding tiltrotor model to properly reflect the design-specific characteristics of this configuration. A description of the convertible engine modeling was discussed earlier in this paper. The changes that were required are as follows.

4.3.1 Wing– The wing weight equations used to size the wing in VASCOMP include aeroelastic terms to avoid whirl flutter, as previously mentioned. To alleviate this phenomenon, a much stiffer wing structure is required, which would result in a higher overall wing weight. Because the folding tiltrotor does not utilize its proprotors for high-speed flight, the wing stiffness required to avoid whirl flutter is greatly reduced. This allows the values for

the torsional, beam, and chord natural frequency ratios for the wing structure to be relaxed, thereby producing a lighter wing. The values used to determine the aeroelastic effects were based on methods developed in reference 23 and correspond to a proprotors-on dive velocity of 320 knots.

4.3.2 Proprotor system– In order to model the folding tiltrotor, adjustments were made to account for the additional weight and drag associated with the blade folding. This includes a 50% weight penalty on the total proprotor system weight for the blade-folding and -stowing mechanism.

In addition to the weight penalty, drag for the stowed blades during cruise must be taken into account. During the jet-thrust mode, the blades are indexed, folded, and stowed against the nacelles, producing a drag penalty for their protrusion into the airstream. During the large-scale wind-tunnel testing of a folding tiltrotor by Bell Helicopter (ref. 30), this protrusion resulted in an incremental C_D of 0.003 based on wing semispan. Based on these data, VASCOMP was modified to include a drag term that scaled with proprotor disk area to account for this additional drag.

5. Optimization

5.1 Design Parameters

For each vehicle, a number of important performance-related design parameters were identified based on the assumptions and modeling described in section 4. The parameters examined are listed as follows:

	Tiltrotor	Tiltwing	Folding tiltrotor
Proprotor			
Disk loading	X	X	X
Hover tip speed	X	X	X
Cruise tip speed	X	X	
Wing			
Wing loading	X		X
Wing c/D		X	
Wing t/c	X	X	X
Wing sweep	X		X
Engine			
Engine, spanwise position		X	
Mission			
Cruise altitude	X	X	X

These parameters were selected because of their large effects on vehicle drag, fuel efficiency, and ultimately the aircraft weight, the key objective function of the sizing optimization.

Inspection of the above matrix of design parameter choices reveals three major differences that need to be explained. First, the wing loading and wing chord-to-propeller diameter (c/D) are two equivalent parameters that size the wing area. Both the tiltrotor and folding tiltrotor use the more conventional parameter of wing loading, while the tiltwing uses c/D as a design variable because of its more direct effect on wing stall during reconversion. Second, the tiltwing was not permitted to sweep its wing because of proprotor and ground clearance problems. Finally, engine spanwise position was chosen as a design variable for only the tiltwing. Since the tiltwing has a structural advantage over the tiltrotors with regard to jump-takeoff requirements, fixed-wing cruise design criteria were predicted to size its wing. If this is the case, allowing the engine to vary its spanwise position might reveal an optimum spanwise location for maximum bending relief and minimum wing weight. For this study, the tiltwing engine position was allowed to vary with no drag penalty to examine the effect of engine position on bending relief.

5.2 Constraints

In the optimization process, constraints must be imposed to keep the vehicle out of unrealistic regions in the design space. For this study, optimization constraints for all concepts included (1) a disk loading limit of 21 lb/ft^2 (as suggested from reference 24) to avoid excessive downwash 360° around the vehicle, (2) a hover tip speed limit of 750 ft/sec to avoid excessive noise, and (3) all of the mission fuel must fit in the wing of the aircraft. One additional concept-specific constraint was the requirement that the selected wing configurations not be subject to wing stall during reconversion for the tiltwing.

5.3 Convergence

The effect of each design parameter, individually and in conjunction with other parameters, on the vehicle's gross weight was then studied. For each design parameter, either an optimum value was found or a practical limit was reached. The optimum vehicle design parameters were determined to a tolerance of ±5% of the optimum value. Finally, the result of the design parameter study was the definition of an optimized vehicle of minimum gross weight. This final, optimized vehicle design was termed the current-technology baseline. A detailed discussion of each baseline vehicle follows.

6. Current-Technology Results

The results of the optimized current-technology version of each of the configurations are detailed in tables 1–4. Table 1 compares the optimum gross weight and design variable choices. Table 2 exhibits general vehicle geometric parameters and performance measures. Table 3 shows a detailed weight breakdown for each vehicle, and table 4 provides the detailed parasite drag breakdown for each of the vehicle types. Comparison of these optimized vehicles follows.

6.1 Design Tradeoffs

The final optimum design variables can be found in table 1. Detailed discussion of the tradeoffs that result in these variable choices was avoided in order to concentrate on the advanced-technology results discussed later in this paper. For the most part, the tradeoffs described in the all-advanced-technology section apply for these vehicles as well.

6.2 Geometry

The most significant geometric differences between the three current-technology vehicles are found in the proprotor, wing, and engine nacelle sizes found in table 2. In order of largest to smallest proprotors are the folding tiltrotor, the tiltwing, and the tiltrotor. Proprotor size was determined by the disk loading and vehicle gross weight. The proprotor of the folding tiltrotor is the largest because of its low (13 lb/ft^2) disk loading, chosen to allow a matching of the hover and cruise engine power. The folding tiltrotor's convertible engine can be hover/cruise matched because of the uncoupling of the proprotor with cruise flight. The demanding 450-knot cruise enforced high required cruise powers on tiltrotors and tiltwings because of their inefficient current-technology proprotors. The tiltwing has the second largest proprotor, a result of a combination of the 21-lb/ft^2 disk loading limit and its large wing and very heavy weight. Finally, the tiltrotor has the smallest proprotor—the result of its high, 21-lb/ft^2 (design limit) disk loading and low aircraft gross weight.

The wing sizes on the three vehicles are significantly different. The tiltwing requires a wing of 1272 ft^2, more than double the size of the folding tiltrotor and four times the size of the tiltrotor wing. The tiltwing needs such a large wing to avoid reconversion stall. This large wing is necessary because of the low disk loading limit required by the mission under study. Historically, tiltwings such as the XC-142 did not run into this problem because of their higher disk loadings.

The folding tiltrotor has the second largest wing because of its need to keep its large proprotors clear of the fuselage after conversion. Finally, the tiltrotor has the smallest optimum wing area due to its small proprotors.

The engine nacelle sizes vary from the 7.0-ft mean diameter for the tiltwing to the small, 5.3-ft-mean-diameter folding tiltrotor nacelle with the tiltrotor having a mid-sized engine nacelle size of 5.8 ft diameter. The tiltwing nacelle is large due to the high engine power required to propel the large wing in cruise. The folding tiltrotor nacelle is the smallest due to the low hover/cruise-matched engine power required.

6.3 Weights

As shown in table 1, the three vehicles have vastly differing gross weights. The heaviest is the tiltwing, weighing 65,367 lb. Next heaviest is the folding tiltrotor with a gross weight of 48,414 lb. The lightest vehicle is the 43,441-lb tiltrotor. The dominant factor in the tiltwing weight is its large wing, discussed above. The gross weight of the folding tiltrotor is higher than that of the tiltrotor due to its heavy convertible engine, its large proprotors with heavy blade-folding mechanisms, and its significantly larger wing.

6.4 Drag

The parasite drag breakdown in table 4 shows that the vehicle with the largest flat-plate drag area is by far the tiltwing, followed by the folding tiltrotor and the tiltrotor. The primary reason for the high drag of the tiltwing is, again, its very large wing. The folding tiltrotor has significantly more flat-plate drag area than the tiltrotor due mostly to its folded-blade drag and large wing area.

7. Advanced Technologies

The assessment of future VTOL designs is based on many ongoing research efforts that promise to enhance various applicable technologies. Many of these advanced technologies will impact the viability of a high-speed rotorcraft. At the conceptual design level, it is important to identify those technologies that will have the greatest impact on future vehicles in order to help guide the focus of the research effort. For each of the high-speed rotorcraft under study, the technology advancements found in table 5 were assumed and the impact of each on the current-technology design was assessed.

The assessment was made by re-optimizing the current-technology vehicle with the projected technology

improvement. During these optimizations, the initial constraints remained in effect.

First, the basis behind the specific advanced-technology projections will be discussed, and then the effects of each of these technologies on the vehicle gross weights and design variables will be examined.

7.1 Technology Projections

7.1.1 Advanced proprotor aerodynamics– The first technology examined was an advanced-technology proprotor. If a V-22-style rotor is used at the high speed of 450 knots, VASCOMP studies predict vehicle cruise efficiencies of roughly 0.5. This level of performance is not adequate for development of an efficient tiltrotor or tiltwing. In their high-speed rotorcraft reports, Boeing, McDonnell-Douglas, and Sikorsky have predicted "current technology" proprotor cruise efficiencies of 0.71, 0.75, and 0.79, respectively (ref. 25). The current-technology proprotor used on the tiltrotor and tiltwing was tailored to achieve cruise efficiencies of around 0.70 for the low, optimized altitudes of the current-technology tiltrotor.

Since the optimized current-technology tiltrotor and tiltwing operate with their proprotors heavily into compressibility, there is an opportunity to improve performance with an advanced-technology proprotor. For example, M_{DD} for the tiltrotor proprotor airfoil at 75% radius equals 0.68, while M_{cruise} (this is not even a helical tip Mach number!) equals 0.72. This study's projection for a next-generation high-speed proprotor is an increase in proprotor airfoil M_{DD} of 0.07. This could be achieved through some method of thinning and/or sweeping the proprotor blades.

7.1.2 Advanced wing and airframe aerodynamics– The application of advanced leading- and trailing-edge devices that will delay wing stall should have a positive effect on the tiltwing. The higher lift provided by this technology allows the tiltwing to utilize smaller wings during reconversion and therefore reduce the gross weight. The technology baseline assumed was a maximum lift coefficient of 3.5 and a stall angle of attack of 22°—which reflects typical double-slotted flap performance. The advanced-technology goal used for this study is an improvement of 0.5 in maximum lift coefficient and an increase of 5° in stall angle of attack. The maximum-lift-coefficient goal of 4.0 represents an evolutionary improvement in passive maximum-lift system performance. This level could be easily attained by a powered-lift scheme, but this would also entail weight and engine air-bleed penalties not considered in this study.

Wing drag divergence is another area that would benefit from advanced technology, specifically the use of advanced, supercritical airfoils. A projected increase in wing M_{DD} of 0.05 above typical supercritical airfoil performance (as defined by ref. 8) was used for this study.

One advanced airframe technology examined was a projected reduction of 10% in the vehicle parasite drag. Current-technology rotorcraft from this study exhibit typical turboprop transport aerodynamic efficiencies (mean skin-friction drag coefficients = 0.041–0.043). Lacking a stated research goal in this area, we chose a 10% reduction in the vehicle parasite drag as a reasonable advance to be pursued.

7.1.3 Advanced propulsion technology– A more fuel-efficient engine would also improve the capabilities of advanced VTOL aircraft. This study used the goal of a 20% reduction in turboshaft engine specific fuel consumption from that found for the baseline GLC38-T1M1 engine. This 20% reduction is based on the stated goal of Phase 1 of the joint DOD- and NASA-sponsored Integrated High-Performance Turbine Engine Technology (IHPTET) program.

IHPTET did not have a fuel-efficiency goal for a convertible engine, so advanced-technology predictions from the engine manufacturer had to be used. Using data from reference 31, a cruise fuel flow reduction of 10% from the baseline GE38/CE4 convertible engine fuel flow was anticipated to be possible.

Another goal of the IHPTET engine technology development program is an increase in the ratio of turboshaft engine power to weight by 40%. Thus, another advanced technology investigated was a 40% increase in turboshaft engine power to weight over that of the baseline GLC38-T1M1 engine.

Again, future convertible engine power advances were not specified by IHPTET, so the engine manufacturers had to be consulted. Reference 31 estimates that the convertible engine power-to-weight and engine thrust-to-weight ratios could both be increased by 17%. Accordingly, this increase in engine power to weight was studied as another advanced technology.

7.1.4 Advanced structures/materials technology– Through careful use of upcoming composite technology, the Army's Advanced Composite Airframe Program (ACAP) for rotorcraft has stated as its goal the reduction of aircraft structural weight from a baseline all-aluminum structure by roughly 20%. This study investigated the effects of a similar 20% reduction in structural weight over that of early-1970s metal structure design.

Another advanced technology considered was a reduction in drive system weight of 20% over that of 1970s metal construction techniques. This is close to the stated 25% goal of the Army's Advanced Rotorcraft Transmission (ART) program. Since the drive system weight is the largest single component weight in the current-technology tiltrotor and tiltwing, significant weight reduction would be expected from the assumption of lighter transmission weights.

7.2 Tiltrotor Results

For the tiltrotor, the impact of the above advanced technologies, both independently and in combination, was examined. For each investigation, the technology was applied to the current-technology baseline and the vehicle was re-optimized. The optimized gross weight was plotted for each technology in figure 5.

The most promising advanced technology for the tiltrotor is the advanced-technology proprotor, which reduces vehicle gross weight by 12%. The use of this advanced proprotor increases the propeller cruise efficiency from 0.68 to 0.76. The most significant changes in the optimum vehicle design parameters are an increase in cruise tip speed from 410 ft/sec to 488 ft/sec and an increase in cruise altitude from 16,800 ft to 22,500 ft. Both parameters increase to take advantage of the higher Mach numbers tolerated by the proprotor without degrading propulsive efficiency. The higher cruise tip speed lessens the drive system weight and the effect of the engine power reduction associated with a significant difference in the hover and cruise tip speeds. The higher altitude lessens the cruise drag through lower dynamic pressure.

In order of decreasing advantage, the rest of the advanced technologies are reduced structural weight, lower specific fuel consumption, lighter drive system weight, increased engine power to weight, and reduced parasite drag. Predicted vehicle gross weight savings from these technology advances ranged from 8% to 4%. These weight savings were the result of direct component or required fuel weight reductions and the impact of cascading weight reduction. In all cases except for the increased engine power to weight, the optimum vehicle design parameters did not change significantly from the current-technology baseline. These optimum design parameters had the following values: disk loading and hover tip speed limited to 21 lb/ft^2 and 750 ft/sec, respectively, cruise tip speeds about 410 ft/sec, wing thickness ratios about 17%, wing loadings around 140 lb/ft^2, no wing sweep, and cruise altitudes about 17,000 ft.

Increasing the turboshaft engine power to weight by 40% resulted in a change of the optimum cruise altitude from 16,800 ft to 18,400 ft. In this case, the higher engine performance allows the more efficient, higher-altitude cruise.

Finally, two technologies that do not show up on figure 5 are the application of advanced leading- and trailing-edge devices and the increase in wing drag divergence. Neither of these technologies significantly changed the gross weight or vehicle design of the current-technology tiltrotor. In the case of the leading- and trailing-edge devices, since this technology improvement only affects the conversion segment of the tiltrotor—which does not size any major vehicle component—it was not expected to affect the tiltrotor. In the case of the wing drag divergence increase, because the current-technology tiltrotor wing operates at a Mach number less than M_{DD}, no significant benefit accrued.

The cumulative effect of all the above technologies was a reduction in the gross weight of 32%. The results of this optimization will be termed the all-advanced-technology tiltrotor; details of the vehicle configuration will be discussed in section 8.1.1.

7.3 Tiltwing Results

The advanced technologies discussed previously were also applied separately and jointly to the tiltwing. In each case the tiltwing was re-optimized. The optimized gross weights are presented in figure 6. The effect of these technologies will now be discussed, as was done previously for the tiltrotor.

As in the case of the tiltrotor, the most significant advanced technology for tiltwings is the advanced-technology proprotor. The improved proprotor reduces the tiltwing gross weight by 33%. The cruise propeller efficiency for the minimum-gross-weight vehicle increases from 0.63 to 0.75.

The improved propeller efficiency drives the cruise tip speed and cruise altitude higher, the wing thickness lower. The increased tip speed improves cruise fuel consumption and reduces drive weight. The higher cruise altitude results in a dramatic improvement in L/D, mainly by allowing operation closer to L/D_{max}. The L/D increase results in lower fuel weight required. Also, as cruise altitude increases, the wing thickness ratio must decrease to avoid wing drag divergence.

The second most significant technology for tiltwings is the advanced wing leading- and trailing-edge devices. The improved wing reduces the gross weight by 19%. The

wing chord/propeller diameter (c/D) decreases from 0.335 for the baseline to 0.235 for the optimized tiltwing.

The reduced c/D decreases the wing chord without changing the span much. This results in reduced wing area and increased aspect ratio. These two changes increase the cruise L/D, which results in less drag and smaller engines.

The optimum wing aspect ratio is much greater (8.27 as opposed to 5.72 for the baseline). The wing weight is not excessive, however, because the reduction in wing area means higher wing loading, which in turn reduces the gust load factor contribution to the wing weight.

As shown in figure 6, the other technologies, in order of decreasing impact on gross weight, are as follows: structural weight reduction, drive weight reduction, reduced sfc, increased power to weight, parasite drag, and increased drag divergence Mach number. These technologies provide reductions in gross weight from 14% down to 8%, with the exception of the increased drag divergence Mach number discussed below. The optimum design variables for the above optimizations are all very similar, with disk loading and hover tip speed limited to 21 lb/ft^2 and 750 ft/sec respectively, cruise tip speeds about 410 ft/sec, wing thickness ratios about 14%, chord-to-diameter ratios about 1/3, cruise altitudes about 27,000 ft, and optimum engine positions near the wing tip.

The reasons for the weight reductions for these technology enhancements can be more directly traced to the technology change than to the improved proprotor or the wing lift and drag improvements. The structural weight, drive weight, and increased power-to-weight ratios are direct weight reductions. The reduced specific fuel consumption reduces the weight of fuel required. The parasite drag reduction reduces both fuel weight and engine size and weight. All weight reductions have a cascade effect on the gross weight of the vehicle.

Increased drag divergence Mach number produced no reduction in gross weight. This is because the effect of wing profile and interference drag keeps the wing thickness-to-chord ratio low enough that the minimum-gross-weight current-technology vehicle cruises well below its wing drag divergence.

The cumulative effect of all the above technologies was a reduction in the gross weight of 54%. The results of this optimization will be termed the all-advanced-technology tiltwing and discussed in section 8.1.2.

7.4 Folding Tiltrotor Results

For the folding tiltrotor, the effects of eight advanced technologies and their combination were also examined. Each technology change generated a different optimized vehicle; the optimized gross weight was plotted for each technology in figure 7. The effects of these changes in technology will now be discussed.

For the folding tiltrotor, the most significant impact on the gross weight was obtained by realizing a reduction in vehicle structural weight. A decrease of 20% in the vehicle structural weight resulted in a total gross weight reduction of nearly 14%.

A listing of the other technologies, starting with the most effective in reducing gross weight and continuing to the least effective, follows: reduced drive system weight, increasing engine power to weight, lower specific fuel consumption, reduced parasite drag, and increased wing drag divergence Mach number. The impact of these technologies was to reduce vehicle gross weights from 5% to 2%. In each advanced-technology case, vehicle gross weight was decreased by direct component or fuel weight savings coupled with the cascading effect of decreasing gross weight.

Even though the advanced technologies affected the gross weight significantly, the optimum vehicle design parameters never varied significantly from those of the current-technology baseline. These optimum design parameters were as follows: hover tip speed limited to 750 ft/sec, 13 lb/ft^2 disk loading, wing thickness ratios of 15%, wing loadings around 82 lb/ft^2, forward wing sweep of 24°, and cruise altitudes of about 39,000 ft.

The last two advanced technologies examined, advanced leading- and trailing-edge devices and the advanced-technology proprotor, had no impact on the folding tiltrotor design optimization. Using an advanced-technology proprotor should provide minimal, if any, improvement for a folding tiltrotor since so little time is spent in hover and conversion for the civil mission. As in the case of the tiltrotor, the application of advanced leading- and trailing-edge devices that significantly help the tiltwing in reconversion did not change the folding tiltrotor's gross weight or vehicle design.

By using each of the advanced technologies in combination and re-optimizing, a gross weight reduction of 25% was realized. The results of this optimization, known as the all-advanced-technology folding tiltrotor, will be discussed in section 8.1.3.

7.5 Comparison

Inspection of the advanced-technology impacts for all three configurations shown in figures 5–7 reveals two major conclusions. First, the application of advanced technologies promises very significant gross weight savings for all high-speed rotorcraft of the future. Gross

weight savings for the all-advanced-technology versions of the tiltrotor, tiltwing, and folding tiltrotor vary from 25% to 55%.

Second, in order of highest to lowest gross weight reduction from the application of advanced technologies are the tiltwing, tiltrotor, and finally the folding tiltrotor. This means that the tiltwing gets the most benefit from the use of the proposed advanced technologies. On the other hand, this also means that the performance of the future tiltwing is the most dependent on the achievement of the advanced-technology goals.

8. All-Advanced-Aircraft Results

The combination of all the advanced technologies discussed were incorporated into each vehicle, and VASCOMP was used to determine the optimum vehicle design. The final design parameters chosen are shown in table 6. Discussion of the design tradeoffs, geometry and performance, weight, drag, and gross weight sensitivity of these all-advanced-aircraft baseline configurations follows.

8.1 Design Tradeoffs

8.1.1 Tiltrotor– The optimized tiltrotor with all the advanced technologies applied weighs 29,441 lb. The final design parameter values for the vehicle are:

Disk loading	21 lb/ft^2
Hover tip speed	742 ft/sec
Cruise tip speed	474 ft/sec
Wing loading	107 lb/ft^2
Wing t/c	0.19
Wing sweep	0°
Cruise altitude	24,800 ft

Detailed discussion of the design tradeoffs involved in the optimum choice of the above design variables follows.

8.1.1.1 Disk loading: For lower disk loading than the optimum 21 lb/ft^2, heavier vehicle designs result from higher wing, proprotor system, drive system, and flight control weights. With a lower disk loading, increased proprotor-system, drive-system, and flight-control weights result from the larger-diameter proprotor. Also, since the proprotor size drives the wing span, lower disk loading increases the wing span and thus increases wing aspect ratio (for fixed-wing loading), driving the wing weight up. The combination of all the above increasing weights drives up the vehicle gross weight.

For disk loadings higher than 21 lb/ft^2, operational considerations limited "high" disk loadings from consideration. When unconstrained optimizations were run, the optimum disk loading went to 45 lb/ft^2. All of the above factors, which drove the vehicle weight heavier with lower disk loading, drive the vehicle weight lighter with higher disk loading. However, to avoid overturning personnel in the proprotor downwash, a downwash limit of 21 lb/ft^2 disk-loading constraint was imposed (ref. 24).

8.1.1.2 Hover tip speed: Lower hover tip speed than the 742 ft/sec optimum gave rise to higher vehicle gross weight through higher required proprotor blade, engine, and drive system weights. The trail of cause and effect begins with proprotor C_T/σ. In order to have sufficient maneuverability, the proprotor C_T/σ is limited to 0.125. At a fixed C_T/σ, decreasing the hover tip speed increases the proprotor C_T, which forces higher blade solidity. This higher blade solidity results in high proprotor blade weight. Furthermore, since the tiltrotor uses the same proprotor for both hover and cruise, the blade solidity affects the cruise power. This increased solidity provides more proprotor blade area than necessary, which leads to lower cruise efficiencies and higher drive system torques. Lower cruise efficiency leads to higher installed engine power and weight; higher drive torques lead to higher drive system weight. The heavier component weights cause an increase in vehicle gross weight.

For higher hover tip speed than the optimum 742 ft/sec, the dominant factors in increasing gross weight become increasing proprotor hub weight and the cruise tip speed/hover tip speed mismatch. First, the proprotor hub weight is sized by the highest value of (Proprotor rpm)^2 * (Power Required) in any of three conditions: hover, conversion, and cruise. For the tiltrotor, the hub is heavily sized by conversion. Since conversion tip speed was set equal to hover tip speed for this study, increasing the hover tip speed drives up the proprotor rpm in conversion. This rpm increase leads to higher proprotor hub weight and, ultimately, higher vehicle gross weight.

Second, with high hover tip speed, the cruise tip speed/hover tip speed mismatch plays a major role in increasing vehicle gross weight. Through reduction by a gearbox, hover tip speed is matched to the design engine turbine speed. Thus, operating the rotor at lower tip speeds, such as for cruise, forces the engine to operate off of its design turbine speed; this results in two major effects: an engine power dropoff and an increase in the engine specific fuel consumption. VASCOMP models the power loss as a quadratic dropoff with off-design turbine speed. Thus, as we increase the hover tip speed while leaving the cruise tip speed fixed, the available cruise

power level will vary with the cruise tip speed/hover tip speed mismatch—the greater the mismatch, the greater the cruise power loss. Likewise, the higher the cruise tip speed/hover tip speed mismatch, the worse the cruise specific fuel consumption becomes, and the higher the cruise segment fuel burn. The subsequent combination of the higher cruise power, which sizes the engine, and the higher cruise segment fuel burn, the most taxing segment in terms of fuel required, results in heavier engine and fuel weights and, subsequently, higher vehicle gross weight.

8.1.1.3 Cruise tip speed: Lower cruise tip speed than the optimum 474 ft/sec increases the gross weight through higher drive system, engine, and fuel weights. Lower cruise tip speed results in higher drive system torques and a bigger mismatch in hover and cruise tip speeds. Drive system weight increases with the higher cruise torque levels. The quadratic power dropoff and worse specific fuel consumption with a higher mismatch in cruise tip speed and hover tip speed yield higher required cruise engine power and cruise fuel flow and thus higher engine and fuel weights. The combination of higher drive system, engine, and fuel weight increases the vehicle gross weight.

Higher cruise tip speed than 474 ft/sec results in higher vehicle gross weight due to higher engine and wing weights. First, at 450 knots, the proprotor airfoil is already encountering significant compressibility drag. Thus, at higher cruise tip speed, the compressibility drag increases steeply and results in lower cruise efficiency. The lower cruise efficiency requires higher installed engine power and weight. Second, the wing weight required to avoid whirl flutter is a strong function of cruise tip speed. This forces higher wing weight as cruise tip speed is increased.

8.1.1.4 Wing loading: For lower wing loading than the optimum 107 lb/ft^2, the main reasons for increasing gross weight were higher engine and drive system weights. Lower wing loading increased the cruise drag significantly, and since the engines and drive system are sized for cruise, the extra drag led to higher cruise power and torque and thus high installed engine and drive system weights.

For higher wing loading than the optimum, a higher wing weight was responsible for increasing gross weight. This fact is not intuitive and produces the paradox of smaller wings with higher wing weights. The reason underlying this paradox is the sizing of the wing for whirl flutter. The aeroelastic whirl flutter problem is aggravated by a high wing aspect ratio. Now, the tiltrotor wing aspect ratio is determined by both wing span and wing chord. Wing span is fixed by disk loading and the separation of the inboard proprotor tips and is thus fixed for varying wing loading. Wing chord, however, is directly determined by the wing loading. Thus, as wing loading increases, the wing area decreases and so does the wing chord. For the optimized tiltrotor wing, the wing weight sizing for whirl flutter is a stronger function of wing aspect ratio than it is for wing area. This results in high wing loadings increasing the wing aspect ratio, which, in turn, increases the wing weight and therefore results in a higher vehicle gross weight.

8.1.1.5 Wing t/c: For wing t/c lower than the optimum 0.19, vehicle gross weight increases due to higher wing weight. Designed for whirl flutter, the wing weight is sensitive to wing thickness, and the lower the t/c, the higher the wing weight.

For higher than optimum wing t/c, higher engine and drive system weights increase the vehicle gross weight. Higher wing thickness leads to increased vehicle cruise drag. The increased cruise drag is not, as one would expect, due to compressibility drag (at 450 knots, 24,800 ft, 0.19 wing thickness keeps M_{DD} above M_{cruise} by 0.02), but rather increased wing profile drag, wing-fuselage interference, and wing-nacelle interference drag. (Interference drag was modeled to increase as $(t/c)^3$ (ref. 11).) The increased cruise drag leads to higher engine power and drive system torque. These in turn lead to higher engine and drive system weights and thus higher vehicle gross weight.

8.1.1.6 Wing sweep: For nonzero wing sweep, heavier wing weight leads to increased vehicle gross weight. Since the wing is not operating into compressibility drag divergence, wing sweep is only detrimental to the vehicle gross weight. For a fixed wing span, the higher the wing sweep, the higher the wing bending moments, and the higher the wing weight. Higher wing weight forces increased vehicle gross weight.

8.1.1.7 Cruise altitude: For lower than the 24,800-ft optimum cruise altitude, vehicle gross weight increases because of higher required drive system weights. The lower altitude leads to higher cruise drag through increased dynamic pressure. Higher cruise drag increased the drive system torque, which in turn increased the drive system weight. Finally, the higher drive system weights led to higher gross weights.

Higher altitude than optimum increased the vehicle gross weight because of two major factors: greater engine and fuselage weights. First, as cruise altitude increases, the local speed of sound, and thus local Mach number, increases. This increase in local Mach number causes higher compressibility drag for the proprotor and thus lower proprotor efficiency. This lower proprotor efficiency, combined with the effect of engine lapse with

altitude, significantly drives up the installed engine power required and engine component weight. Higher engine weight results in higher vehicle gross weight.

Second, higher cruise altitude yields heavier gross weights because of the effect of increased fuselage weight. The fuselage weight increases because the fuselage cabin is required to be pressurized to maintain an 8,000-ft pressure level. Higher altitude requires elevated levels of fuselage pressurization and thus increased fuselage weight. Higher fuselage component weight increases the total vehicle gross weight.

8.1.2 Tiltwing– The tiltwing with all the advanced technologies applied weighs only 29,438 lb. The design variables which produce this minimum gross weight are listed below.

Disk loading	21 lb/ft^2
Hover tip speed	750 ft/sec
Cruise tip speed	440 ft/sec
Wing c/D	0.244 lb/ft^2
Wing t/c	0.15
Engine, spanwise position ($2 * y_{engine}$/wing span)	0.814
Cruise altitude	42,900 ft

Detailed discussion of the design tradeoffs involved in the optimum choice of the above design variables will be described in separate sections below.

8.1.2.1 Disk loading: The disk loading is constrained at the maximum downwash limit of 21 lb/ft^2. Like the tiltrotor, the unconstrained optimum tiltwing disk loading would be higher because of the resulting lower proprotor system, drive system, flight control, and wing weights.

8.1.2.2 Hover tip speed: For noise considerations, the hover tip speed is constrained at the maximum allowed 750-ft/sec tip speed. The optimum hover tip speed is higher than this because of the connection between hover tip speed and solidity for a fixed C_T/σ. This connection was explained before for the tiltrotor. In brief, higher hover tip speeds yield lower proprotor solidity. This lower proprotor solidity generates higher propeller efficiencies, which result in lower engine power and drive torque. In turn, lower engine power and drive torque result in lower engine and drive system weights and thus gross weight.

8.1.2.3 Cruise tip speed: The optimum cruise tip speed occurs at a sizing corner for wing weight. A sizing corner is a design point where two or more constraints are imposed at the same time. If the cruise tip speed is reduced from the optimum, the wing is sized by cruise bending moment. However, the reduction in tip speed increases the transmission weight, and the gross weight increases. If the cruise tip speed is increased from the optimum, the wing is sized by whirl flutter, and the wing weight increases faster than the transmission weight decreases. Therefore, the overall gross weight increases if the cruise tip speed is varied from the optimum.

8.1.2.4 Wing chord/propeller diameter (c/D): For the current-technology wing, there is a tradeoff between avoiding stall during reconversion and having a poor L/D with an oversized wing. In the case of the all-advanced-technology wing, however, the reconversion stall is not critical. The optimum is a tradeoff between wing weight and cruise drag. If the c/D ratio is decreased from the optimum, the aspect ratio increases and the wing, now sized by whirl flutter, increases rapidly in weight. If the c/D ratio is increased from the optimum, the wing is sized by bending moment, and the wing weight increases because of size and increased gust load factor caused by the reduction in wing loading. Also, the aircraft drag increases because of the increased wetted area of the wing and increased interference drag.

8.1.2.5 Wing t/c: The optimum wing t/c reflects a tradeoff between wing weight and wing drag. If the thickness is reduced from the optimum, the wing weight increases because the spar depth is reduced. If the thickness is increased from the optimum, the wing drag form factor and interference drag increases, which in turn increases the aircraft drag, engine size, and fuel consumption. These increases in weight are greater than the reduction in wing weight due to the increased spar depth.

8.1.2.6 Engine, spanwise position: The optimum engine spanwise position is selected by a tradeoff between wing sizing by bending and wing sizing by whirl flutter. If the engine is inboard of the optimum, the bending relief provided by the engine is decreased and the wing is increasingly sized by bending moment. If the engine is outboard of the optimum, the wing is sized by whirl flutter. As mass is moved outboard, the torsional stiffness is decreased, so the wing weight increases.

8.1.2.7 Cruise altitude: The optimum cruise altitude is determined by a complicated tradeoff involving engine weight, wing drag divergence, and cruise L/D. If the cruise altitude is increased from the optimum, two things happen which increase the weight. The first is that the engine weight increases because of the lapse rate with altitude even if the power required decreases. The second

is that the cruise drag divergence Mach number decreases because of increasing lift coefficient that results from decreasing air density. Note that the cruise Mach number does not increase at constant TAS above 36,000 ft (as it did below 36,000 ft) because the temperature is constant there. If the altitude is decreased from the optimum, the L/D decreases due to higher drag from the increasing dynamic pressure.

8.1.3 Folding tiltrotor– The optimized folding tiltrotor weighs 36,337 lb. The final design parameter values for the optimized vehicle are:

Disk loading	14 lb/ft^2
Hover tip speed	750 ft/sec
Wing loading	85 lb/ft^2
Wing t/c	0.15
Wing sweep	–20°
Cruise altitude	41,000 ft

Discussion of the design tradeoffs involved in the optimum design variable choices follows.

8.1.3.1 Disk loading: For lower disk loading than the optimum 14 lb/ft^2, higher gross weight results from higher wing, proprotor, drive, and flight-control component weights. First, higher aspect ratio increases the wing weight. For a fixed wing area, lower disk loading increases the required wing span and results in higher aspect ratios. This higher aspect ratio increases the wing weight because of a need to design for a higher gust load. Since the folding tiltrotor wing is sized by cruise bending moment, gust loading becomes the major factor in determining the wing weight. Second, the proprotor weight increases because of the larger proprotor that results from lower disk loading. Last, given the larger proprotor size, the drive system and flight control weight necessary for the heavier proprotor increases. When these higher component weights are incorporated into the vehicle, the vehicle gross weight increases.

Increasing the disk loading higher than the 14-lb/ft^2 optimum increases vehicle gross weight through higher engine weight. This engine weight increases because, for a higher disk loading, the engine is sized by hover. Since a smaller proprotor has lower thrust-to-power ratio, higher disk loadings require higher engine powers to hover. This higher engine power results in heavier engine weight and, finally, higher vehicle gross weight.

8.1.3.2 Hover tip speed: Like the tiltwing, the folding tiltrotor's optimum hover tip speed was limited by the 750-ft/sec noise constraint. The optimum tip speed is higher than the limit because of the beneficial effect of lower blade solidity. As previously discussed in section 8.1.1, a fixed C_T/σ of 0.125 causes decreased blade solidity for an increase in hover tip speed. This lower blade solidity results in four separate component weight reductions. First, smaller-solidity proprotor blades weigh less. Second, the drive system required to drive the smaller proprotor blades will weigh less. Third, the lower-solidity proprotor will reduce the amount of folded-proprotor surface immersed in the airstream. This results in lower cruise drag, which leads to less powerful, lighter engines and lower total fuel burned. The combination of lighter proprotor, drive, engine, and fuel weights result in lower vehicle gross weights for hover tip speeds higher than 750 ft/sec. However, the critical factor of noise limits the hover tip speed for the folding tiltrotor.

8.1.3.3 Wing loading: A wing loading lower than the optimum 85 lb/ft^2 increases vehicle gross weight primarily because of higher engine and drive system weights. Lower wing loading translates to a larger wing area for a given weight. A larger wing area results in increased flat-plate drag area and a lower cruise L/D. This increase in cruise drag leads to higher cruise power and torque requirements. Since both the engine and transmission are sized for cruise, this leads to both heavier engines and a heavier drive system required for the folding tiltrotor. These two factors, along with increased structural weights (wing and horizontal tail), lead to a trend of increased vehicle weight as the wing loading decreases.

A higher wing loading than optimum causes a higher vehicle gross weight through increased engine and wing weights. For a fixed disk loading, a higher wing loading leads to a smaller wing area and an increased aspect ratio. First, smaller wing area leads to increased engine weight. As a consequence of the smaller wing, the hover download on the vehicle decreases and the speed necessary for conversion increases. The engine power necessary to convert increases and now becomes the engine sizing condition. As a result, the engine system weight increases. Second, the higher aspect ratio increases up the wing weight. For a higher aspect ratio, the wing weight sizing becomes dominated by whirl flutter. This requires more structural stiffness in the wing and leads to increased wing weight. Taken together, these engine and wing effects lead to an increasing vehicle weight with increasing wing loading.

8.1.3.4 Wing t/c: A wing t/c lower than 0.15 increases the vehicle gross weight through higher wing

weight. Thinner wings result in higher bending loads and thus higher required wing weight.

Wing t/c higher than 0.15 increases vehicle gross weight from the combination of higher engine and fuel weights. Three drag mechanisms increase with higher t/c: wing-fuselage interference, wing-nacelle interference, and wing profile drag. Thus, higher t/c leads to increased cruise drag. This increased cruise drag leads to a higher engine power required and a higher fuel burn. Finally, these factors lead to higher engine and fuel weights.

8.1.3.5 Wing sweep: The 22° optimum wing sweep results from a tradeoff involving wing weight. A lower wing sweep increases the wing weight through a higher gust load factor. A higher wing sweep increases the wing weight through a higher structural span. In the middle, an optimum wing sweep exists which minimizes the wing weight and vehicle gross weight.

8.1.3.6 Cruise altitude: Lower cruise altitude than the optimum 41,000 ft increases the gross weight because of higher required fuel weights. As cruise altitude is decreased, the dynamic pressure increases and leads to higher cruise drag. The higher thrust required to overcome the increased cruise drag results in higher fuel flow rate. The higher fuel flow rate in cruise increases the total fuel required for the mission, and, ultimately, this leads to increasing vehicle gross weight.

Also, a higher cruise altitude than optimum leads to higher vehicle gross weights, but due to increased engine weight. At a higher altitude, the thrust loss due to engine lapse rate increases the engine power required and, thus, the engine weight. This effect cascades into a higher vehicle gross weight.

8.2 Geometry and Performance

Three-view drawings of the vehicles in their respective cruise configurations are shown in figures 8(a)–8(c). The most visually striking differences among the three vehicles are: (1) the stowed proprotor of the folding tiltrotor as opposed to the operating proprotors of the tiltrotor and tiltwing, (2) the zero wing sweep for the tiltrotor and tiltwing, 22° of forward sweep for the folding tiltrotor, and (3) the tiltwing wing extensions necessary for alleviation of the reconversion stall problem.

Detailed performance data for the three configurations are tabulated in table 7.

8.3 Weight

A detailed weight breakdown for all three vehicles is tabulated in table 8. These results are also plotted in figure 9, which highlights the major weight differentiators.

The tiltrotor and tiltwing are the lightest vehicles, both weighing about 29,400 lb, while the folding tiltrotor weighs 36,300 lb.

A close look at figure 9 reveals that even though the tiltrotor and tiltwing have similar gross weights, the component weights show some significant differences. With its larger wing and engines, the tiltwing has higher wing and engine component weights than the tiltrotor. The required wing is larger to avoid reconversion stall and the required engine is larger due to engine lapse effects of the high cruise altitude.

Conversely, the tiltrotor has higher proprotor weight, flight control weight, and fuel weight than does the tiltwing. The higher proprotor and flight control weights derive from the assumption that the tiltrotor weights follow historical helicopter articulated rotor weight trends. The tiltwing proprotor and flight control component weights are based on a database of tiltwing propeller and control weights. Tiltwing propeller and their associated control weights have been historically lower because of the lack of cyclic control. In this study, the tiltwing uses a geared flap-control system to avoid the necessity of cyclic control. The higher fuel weight required for the tiltrotor results from the higher dynamic pressures and thus drag experienced at the lower cruise altitudes flown by the tiltrotor.

The folding tiltrotor weighs about 7,000 lb more than either the tiltrotor or the tiltwing. The two main reasons for this significant weight difference are (1) the convertible engine and (2) the heavy proprotor system and flight controls. The first reason, the convertible engine, increases the gross weight by being heavy and fuel inefficient. For an equivalent power output, the convertible engine is much heavier than a turboshaft engine. Therefore, even though the engine power required is the least (see table 7) for the folding tiltrotor among the three concepts, the engine group (engine wt + nacelle wt + installation wt) is the heaviest. Moreover, this convertible engine is not only heavier, but also less fuel efficient than a comparable turboshaft engine. This results in higher required fuel weight.

The second reason is that the folding tiltrotor has the heaviest proprotor and flight controls weights of the three vehicles. This is not only because these proprotors have the largest diameter, but they also have a 50% weight penalty due to a required blade folding mechanism.

8.4 Drag

A detailed cruise drag breakdown of the three vehicles is tabulated in table 9. These results are also plotted in figure 10, highlighting the major drag differentiators.

In order of increasing flat-plate drag area are the tiltrotor, tiltwing, and folding tiltrotor with, respectively, 12.19, 15.87, and 18.23 ft^2 of flat-plate drag area.

The tiltwing has a significantly higher flat-plate drag area than the tiltrotor for three main reasons. First, the wing, sized to avoid reconversion stall, is larger than that of the tiltrotor. Second, the larger tiltwing engine is housed in a correspondingly larger nacelle. Finally, the higher cruise altitude of the tiltwing produces significantly higher induced drag. Since the dynamic pressure is lower, the wing C_L increases as does the induced drag.

The folding tiltrotor has the highest flat-plate drag area of the three. Its cruise drag is significantly affected by the folded blades and by higher induced drag. The high folded-blade cruise drag results from the large optimum proprotor size. The higher induced drag results from a combination of the high cruise altitudes similar to those of the tiltwing (~40,000 ft) and a low wing aspect ratio similar to that of the tiltrotor (~5.5).

For all three concepts, the wing compressibility drag is very low or negligible. This is evidence that the optimizer is manipulating design variables to avoid significant compressibility drag. Since compressibility steeply increases drag, a vehicle design entering this region of the design space would result in a high gross weight.

8.5 Gross Weight Sensitivities

Since detailed design considerations may identify additional limits on the optimized design parameters discussed above, a sensitivity of the vehicle gross weight to off-optimum design parameter choices is of interest. For each of the advanced tiltrotor, tiltwing, and folding tiltrotor, sensitivity of the vehicle gross weight to changes in each of the design variables was studied. Sensitivity plots of percent change in gross weight versus percent change in design variable for the three concepts can be found as figures 11–13. In each of the figures, line segments are used to allow the reader to follow the design parameter trends and not to represent the actual functions, some of which are discontinuous in slope. Discussion of these sensitivity results follows for each aircraft.

8.5.1 Tiltrotor– Figure 11 shows that the advanced tiltrotor is very insensitive to changes in its optimized design variables. Twenty percent increases and decreases in the design hover tip speed, wing loading, wing t/c, and cruise altitude all produce gross weight changes of less than 1%. The most sensitive design variable is the proprotor cruise tip speed, which still generates gross weight increases of only 3.5% with a 20% change from its optimum value.

8.5.2 Tiltwing– Figure 12 shows that the advanced tiltwing gross weight is more sensitive to its design variables than the advanced tiltrotor. Except for the engine location, twenty percent changes in each design variable produces gross weight changes of more than two percent. The most sensitive design variables are the proprotor cruise tip speed and cruise altitude which generate increases in the gross weight of 4.1% and 5.1%, respectively, with 20% changes from their optimum values.

8.5.3 Folding tiltrotor– Figure 13 shows that the advanced folding tiltrotor gross weight is the most sensitive to design variable changes of any of the three vehicles. The most sensitive design variables are the wing loading and the cruise altitude, which generate increases in the vehicle gross weight of 5.8% and 21.3%, respectively, with 20% changes from their optimum values.

9. Disk Loading Trends

The previous optimization results have presumed the requirement to avoid overturning ground personnel. Since certain civil operations might allow a relaxation of these requirements (e.g., restricting ground personnel to approach from a 90° or 270° azimuth), the effect of higher disk loading limits on the gross weight of the tiltrotor and tiltwing was studied. The results are shown in figure 14. The results of optimizing the folding tiltrotor disk loading were already reported in section 8.1.3.1.

Relaxing the 21-lb/ft^2 disk loading limit for the tiltrotor results in a maximum weight savings of 1800 lb for an optimum 45-lb/ft^2 disk loading. Removing the disk loading limit for the tiltwing results in a maximum weight savings of 3000 lb for a higher 75-lb/ft^2 optimum disk loading.

In both cases, the optimum disk loading resulted from a tradeoff involving engine, wing, and drive weights. For both 21-lb/ft^2 disk loading aircraft, each had an engine that was heavily cruise-sized. Higher disk loading reduces the cruise power and torque requirements as well as the size of the wing, resulting in lower engine, drive, and wing weights. As disk loading increases, however, the hover power required increases. At some disk loading, the hover power sizes the engine. For even higher disk loadings, the engine weight increases as the hover power increases. The optimum vehicle in both cases has a disk loading where the hover-sized engine weight increase

balances the corresponding decrease in wing and drive weights.

Even though both aircraft exhibit an optimum disk loading for the same reasons, this does not explain the wide discrepancy between tiltrotor and tiltwing optimum disk loadings: 45 lb/ft^2 and 75 lb/ft^2, respectively. This discrepancy results from their different download characteristics. Since the tiltrotor has a fixed wing, it experiences a significant download during hover (10% of the gross weight for a 21-lb/ft^2 disk loading case). The tiltwing, however, inclines its wing parallel to the proprotor wake, thereby generating a very small download equal to the washed wing drag (0.6% of the gross weight for the 21-lb/ft^2 disk loading case). The lighter tiltwing download increases the disk loading at which required hover power surpasses the cruise power; it thus increases the optimum tiltwing disk loading over that of the tiltrotor.

10. Speed Trends

10.1 Gross Weight vs. Cruise Speed

In order to study the effect of cruise speed on the weight of the three configurations, the tiltrotor, tiltwing, and folding tiltrotor were optimized for minimum gross weight for cruise speeds varying from 350 to 475 knots. The variation of gross weight with cruise speed for the three configurations is plotted in figure 15.

Inspection of the figure reveals that the tiltrotor and tiltwing have similar gross weights throughout the speed range. For both vehicles, the gross weight increases significantly with increasing cruise speed. The main factor in this steadily increasing gross weight is the reduced proprotor efficiency due to compressibility on the proprotor with increasing forward speed.

Unlike the other concepts, the folding tiltrotor gross weight stays relatively constant. Since the proprotor is uncoupled from the cruise flight, the engine is sized for a hover-cruise power match. For the speed range in question, the engine was always sized by hover, not cruise, so this major driver in the gross weight of the vehicle stayed relatively constant, and thus so did the gross weight.

Finally, inspection of the trends reveals that the tiltrotor and tiltwing are significantly lighter than the folding tiltrotor in the 350–475-knot cruise speed range examined. Furthermore, the magnitude of the weight difference decreases with increasing cruise speed such that all three vehicles approach the same gross weight in the 475–500-knot speed range.

The main reason for the convergence of the gross weight for the three concepts is a combination of the heavy proprotors and convertible engine of the folding tiltrotor with the inefficient proprotor of the tiltrotor and tiltwing. At 350–475 knots, the folding tiltrotor weight is penalized by its large and heavy 14-lb/ft^2 proprotors and by its heavy and fuel-inefficient convertible engine. For speeds increasing from 350 knots, the tiltrotor and tiltwing weight approaches that of the folding tiltrotor due to the worsening problem of proprotor compressibility.

10.2 Productivity vs. Cruise Speed

In addition to weight, one figure of merit frequently used to measure overall vehicle efficiency is productivity. For this study productivity was defined by:

$$\text{Productivity} = \frac{\text{Payload} * \text{Block speed}}{\text{Empty weight}}$$

All three advanced configurations were optimized for maximum productivity for a range of cruise speeds of 350 to 475 knots. The results are shown in figure 16.

Both the tiltrotor and tiltwing yield similar productivity trends with increasing cruise speed. For both configurations, an optimum productivity of about 120 n. mi./hr occurs near a cruise speed of 425 knots. For lower cruise speeds, productivity is decreased by the lowering block speeds. For higher cruise speeds, rapidly increasing vehicle empty weight decreases the productivity. The empty weight increase approximates the gross weight increase found in the last section and occurs for the same reasons (increasing proprotor compressibility leading to higher cruise power required, leading to higher engine weights, etc.).

For the cruise speed range examined, the folding-tiltrotor productivity trend shows that the higher the cruise speed, the higher the productivity. As with the gross weight, the folding tiltrotor empty weight is approximately constant throughout the 350–475-knot speed range. Thus, the increasing block speed with cruise speed becomes the major factor in increasing productivity.

The magnitude of the folding tiltrotor productivity is significantly lower than those of the tiltrotor or tiltwing because of its higher empty weight. This higher empty weight is primarily due to the heavy proprotor and convertible engine previously discussed.

10.3 Direct Operating Cost vs. Cruise Speed

Finally, direct operating cost was investigated as an objective function. Direct operating cost is a frequently used economic figure of merit to measure all costs directly involved with the day-to-day operation of a particular vehicle.

In order to calculate direct operating cost, the method of reference 32 was incorporated into the VASCOMP methodology. All three configurations were then re-optimized for cruise speeds between 350 and 475 knots with direct operating cost as the objective function. The results are shown in figure 17.

As with the gross weight and productivity optimizations, the tiltrotor and tiltwing showed the same trend, with an optimum direct operating cost of 12.5 cents/(aircraft seat-mile) at a cruise speed of 425 knots. Slower cruise speeds increase the block time, which is a major factor in increasing most aspects of the direct operating cost, especially the calculation of crew, insurance, depreciation, and interest costs. Higher cruise speeds increase the engine cruise power, proprotor and drive system weights, and fuel weight. These factors figure prominently in the calculation of higher engine, dynamic system, and fuel costs.

Unlike the other two configurations, the folding tiltrotor exhibits direct operating costs that only keep decreasing with increasing cruise speed. This trend results from a combination of the decreasing block time and generally constant engine power and vehicle component weights as the cruise speed increases. Over the speed range examined, the biggest factors in decreasing direct operating cost were the crew, insurance, maintenance burden, depreciation, and interest costs—all decreased by diminishing block time.

11. Concluding Remarks

The results of this study have identified a number of vehicle design trends involving future tiltrotors, tiltwings, and folding tiltrotors. If the advanced-technology goals proposed are achieved, the following conclusions may be made.

First, future low-downwash, high-speed proprotor-driven aircraft will have payload ratios comparable with those of current fixed-wing commercial aircraft. Currently, the Embraer Brasilia 120 and Dornier 328, both 30-passenger turboprops, have payload ratios (ratio of payload weight to gross weight) around 0.20. Both the 450-knot tiltrotor and tiltwing designs have similar payload ratios.

Second, the tiltrotor and tiltwing designs will be lighter than that of the folding tiltrotor. The main reasons for this are heavier and less fuel efficient convertible engine and the large, low disk loading proprotor with its heavy blade-folding mechanism.

By far the most sensitive to the advanced technologies is the tiltwing. The combined effect of all of the advanced technologies on the vehicle gross weight was a savings of more than 50% from the current-technology design. Future tiltrotor and folding tiltrotor designs were somewhat less sensitive than that of the tiltwing, but both saved significant weight from the application of advanced technologies—respective weight savings of 32% and 25%.

The most promising advanced technology for the tiltrotor and tiltwing is a high-efficiency proprotor. Avoiding the use of a proprotor during cruise, the folding tiltrotor achieves its highest weight savings from the application of lightweight materials to its main structural members (e.g., wing, fuselage, nacelle).

The sensitivity of the minimum vehicle gross weight to off-optimum design variable choice ranged from sensitive to very insensitive. In order of most to least sensitive were the folding tiltrotor, tiltwing, and tiltrotor. The folding tiltrotor gross weight increased as much as 21% for a change in design variable of 20%, while the tiltrotor gross weight increased less than 2% for 20% changes in most of the design variables.

Finally, optimizing the three advanced configurations for minimum gross weight, maximum productivity, and minimum direct operating cost for cruise speeds of 350 to 475 knots showed interesting trends. For all three figures of merit, there was no significant difference between the tiltrotor and tiltwing results, but the folding tiltrotor displayed higher gross weight and direct operating cost, and lower productivity.

The gross weight optimizations resulted in a flat trend for the folding tiltrotor and progressively steeper gross weight growth with speed for the tiltrotor and tiltwing. These trends were driven mostly by the engine sizing. Uncoupling the proprotor from the cruise segment of the mission, the folding tiltrotor's convertible engine was sized by hover, and thus unaffected by the cruise speeds in question. On the other hand, the tiltrotor and tiltwing use their proprotor for high-speed propulsion and are forced to compensate for the worsening proprotor compressibility problem through higher installed engine powers. Heavy proprotor and convertible engine weights drive the higher overall gross weights of the folding tiltrotor over those of the tiltrotor or tiltwing.

Both the productivity and direct operating costs show similar trends for the three configurations. For the tiltrotor and tiltwing, maximum productivity and minimum direct operating cost occur at a cruise speed of about 425 knots. Lower cruise speeds result in higher block times, which slightly decrease productivity and increase direct operating cost. Higher cruise speeds increase the vehicle component weights, which result in lower productivity and higher direct operating cost. On the other hand, the folding tiltrotor, with component weights relatively independent of the cruise speeds investigated, is only affected by block time differences. The block time trend results in monotonically increasing productivity and decreasing direct operating cost for the folding tiltrotor.

References

1. DeTore, Jack; and Conway, Scott: Technology Needs for High-Speed Rotorcraft(3). NASA CR-177592, October 1991.
2. Wilkerson, J. B.; Schneider, J. J.; and Bartie, K. M.: Technology Needs for High-Speed Rotorcraft(I). NASA CR-177585, May 1991.
3. Rutherford, J.; O'Rourke, M.; Martin, C.; Lovenguth, C.; and Mitchell, C.: Technology Needs for High-Speed Rotorcraft. NASA CR-177578, April 1991.
4. Scott, M.: Technology Needs for High-Speed Rotorcraft(2). NASA CR-177590, August 1991.
5. Guerrero, L. M.; and Corliss, L. D.: Handling Qualities Results of an Initial Geared Flap Tilt Wing Piloted Simulation. SAE Paper No.-911201, 1991.
6. Schoen, A. H.; Rosenstein, H.; Stanzione, K. A.; and Wisniewski, J. S.: User's Manual for VASCOMP II, The V/STOL Aircraft Sizing and Performance Computer Program (3rd Revision). NASA Contract No. NAS 2-3142, May 1980.
7. Shevell, R. S.: Fundamentals of Flight (2nd edition). Prentice Hall, Englewood Cliffs, 1989.
8. Shevell, R. S.; and Bayan, F. P.: Development of a Method for Predicting the Drag Divergence Mach Number and the Drag Due to Compressibility for Conventional and Supercritical Wings. Stanford University, July 1980.
9. Jacobs, Eastman N.; and Ward, Kenneth E.: Interference of Wing and Fuselage from Tests of 209 Combinations in the N.A.C.A. Variable-Density Tunnel. NACA Report No. 540, 1935.
10. McLellan, Charles H.; and Cangelosi, John I.: Effects of Nacelle Position on Wing-Nacelle Interference. NACA TN-1593, 1948.
11. Hoerner, Sighard F.: Fluid-Dynamic Drag: Practical Information on Aerodynamic Drag and Hydrodynamic Resistance, 1965.
12. Blohm, R.; and Bartie, K.: V-22 Aerodynamic Report. FSCM No. 62851, Number 901-909-632, Bell-Boeing, July 1986.
13. Boeing Helicopters: Investigation of the Performance of Low Disc Loading Tilt Rotors in Hovering and Cruise Flights: Volume I. Analysis and Results. D160-10013-1, March 1971.
14. Felker, F.: Results from a Test of a 2/3-Scale V-22 Rotor and Wing in the 40- By 80-Foot Wind Tunnel. 47th Annual Forum Proceedings of the American Helicopter Society, Volume I, Phoenix, Arizona, May 6-8, 1991.
15. Talbot, P. D.; Bowles, J. V.; and Lee, H. C.: Helicopter Rotor and Engine Sizing for Preliminary Performance Estimation. AIAA Paper 86-1756, 1986.
16. Sanders, Newell D.: Performance Parameters for Jet-Propulsion Engines. NACA TN-1106, July 1946.
17. Hirschkron, R.; and Hull, P.: Convertible Engine System for High-Speed Rotorcraft. AIAA/SAE/ASME/ASEE 26th Joint Propulsion Conference, AIAA Paper 90-2512, July 16-18, 1990.
18. Lindsay, H.; Hirschkron, R.; et al.: Precursor Convertible Engine Study. NASA Contract NAS 3-25460 Final Report, GE Aircraft Engines, November 1989.
19. Schmidt, A. H.; and Dyess, S. B.: Tilt Rotor Wing Weight Estimation. SAWE Paper No. 1926, 1990.
20. Fletcher, R.; and Reeves, C. M.: Function Minimization by Conjugate Gradients. British Computer Journal, vol. 7, no. 2, 1964.

21. Thompson, P.; Neir, R; Reber, R.; Scholes, R.; Alexander, H.; Sweet, D.; and Berry, D.: Civil Tiltrotor Missions and Applications Phase II: The Commercial Passenger Market-Summary Final Report. NASA CR-177576, February 1991.

22. MacWilkinson, D. G.; Blackerby, W. T.; and Paterson, J. H.: Correlation of Full-Scale Drag Predictions with Flight Measurements on the C-141A Aircraft – Phase II, Wind Tunnel Test, Analysis, and Prediction Techniques – Volume 1 – Drag Predictions, Wind Tunnel Data Analysis and Correlation. NASA CR-2333, February 1974.

23. Johnson, W.; Lau, B.; and Bowles, J.: Calculated Performance, Stability, and Maneuverability of High-Speed Tilting-Prop-Rotor Aircraft. 12th European Rotorcraft Forum, September 22-25, 1986.

24. Wernicke, R. K.: Prediction of Tilt Rotor Outwash. AIAA 19th Aerospace Sciences Meeting, St. Louis, Missouri, January 12-15, 1981.

25. Talbot, Peter D.: High Speed Rotorcraft: Comparison of Leading Concepts and Technology Needs. AHS 47th Annual Forum, Phoenix, Arizona, May 1991.

26. Davis, S. J.; and Wisniewski, J. S.: User's Manual for HESCOMP, The Helicopter Sizing and Performance Computer Program. NASA CR-152018, September 1973.

27. Morris, J.; and Ashford, D. M.: Fuselage Configuration Studies. SAE National Aeronautic Meeting, New York, New York, April 24-27, 1967.

28. Talbot, P.; Phillips, J.; and Totah, J.: Selected Design Issues of Some High-Speed Rotorcraft Concepts. AIAA/AHS/ASEE Aircraft Design, Systems and Operations Conference, AIAA Paper 90-3297, September 17-19, 1990.

29. Churchill, G. B.: Free Floating Wing Structure and Control System For Convertible Aircraft. U.S. Patent No. 3,029,043. April 10, 1962.

30. Final Report – Task II Large Scale Wind Tunnel Investigation of a Folding Tilt Rotor. NASA CR-114464, Bell Helicopter Company, May 1972.

31. D'Angelo, M.: High Speed Rotorcraft Propulsion Follow On Study. NASA Contract NAS3-25951 Oral Report, GE Aircraft Engines, June 1991.

32. Duvivier, J. F.; Albertini, F.; Friedlander, S.; Levy, E.; and Peranteau, J.: Methodology for the Evaluation of Intercity and Intraurban V/STOL Transportation Systems. NASA CR-114668, Boeing Vertol Company, July 1973.

Table 1. Current-technology results: optimization results

	Tiltrotor	Tiltwing	Folding tiltrotor
Gross weight, lb	43,441	65,367	48,414
Design variables			
Disk loading, lb/ft^2	21	21	13
Hover tip speed, ft/sec	750	750	750
Cruise tip speed, ft/sec	410	403	N/A
Wing loading, psf	137.5	51.4	81.7
Wing thickness/chord	0.169	0.14	0.150
Wing chord/propeller diameter	0.191	0.335	0.210
Quarter chord sweep, deg	0	0	–24.3
Engine spanwise position (2 * y_{eng}/wing span)	1.0	1.0	1.0
Cruise altitude, ft	16,800	27,200	39,400

Table 2. Current-technology results: geometry and performance

	Tiltrotor	Tiltwing	Folding tiltrotor
Gross weight, lb	43,441	65,367	48,414
Engine			
Sizing condition	Cruise	Cruise	Hover
Maximum power, hp	19,051	38,529	12,987
Nacelle mean diameter, ft	5.8	7.0	5.3
Transmission			
Sizing condition	Cruise	Cruise	Conversion
Maximum torque, ft-lb	145,311	261,095	95,756
Proprotor			
Disk loading, lb/ft^2	21	21	13
Diameter, ft	36.3	44.5	48.7
Solidity	0.132	0.132	0.082
Wing			
Sizing condition	Whirl flutter	Bending	Bending
Wing loading, lb/ft^2	137.5	51.4	81.7
Planform area, ft^2	316	1272	592
Span, ft	45.6	85.3	58.0
Aspect ratio	6.58	5.72	5.68
t/c	0.17	0.14	0.15
c/4 sweep, deg	0	0	–24.3
c/D	0.191	0.335	0.210
Cruise conditions			
Cruise L/D	7.85	8.64	11.16
Proprotor efficiency	0.68	0.63	N/A

Table 3. Current-technology results: weight breakdown

Weight, lb	Tiltrotor	Tiltwing	Folding tiltrotor
Structural weight	8,784	16,631	11,231
Wing	2,390	7,013	3,065
Horizontal tail	367	998	521
Vertical tail	298	449	336
Fuselage	3,240	3,972	3,679
Landing gear	1,303	1,961	1,452
Nacelle	1,186	2,238	2,177
Propulsion weight	12,435	22,546	15,953
Proprotor system	3,069	2,835	5,703
Blade wt/proprotor	472		671
Hub wt/proprotor	1,063		1,230
Blade fold/proprotor	N/A		951
Drive system	5,569	12,830	4,211
Engine	2,636	4,973	4,839
Engine installation	369	696	677
Fuel system	792	1,212	523
Flight controls weight	3,448	3,599	4,903
Fixed equipment	4,800	4,800	4,800
Weight empty (WE/WG)	29,467 (0.68)	47,576 (0.73)	40,887 (0.84)
Fixed useful load	775	775	775
Payload	6,000	6,000	6,000
Fuel	7,199	11,016	4,752
Gross weight (WG)	43,441	65,367	48,414

Table 4. Current-technology results: cruise drag breakdown

Equivalent flat-plate area, ft^2	Tiltrotor	Tiltwing	Folding tiltrotor
Wing	3.01	10.27	5.13
Fuselage	2.97	2.97	2.97
Horizontal tail	0.91	3.35	1.49
Vertical tail	0.72	0.72	0.72
Engine nacelle	2.29	3.29	1.96
Interference			
Wing-fuselage	0.23	0.61	0.32
Wing-nacelle	0.24	1.30	0.35
Folded blades	N/A	N/A	1.43
Miscellaneous	0.76	1.24	0.90
Total parasite drag	11.13	23.74	15.27
Induced drag	2.31	2.62	8.29
Compressibility drag	0.04	0.00	0.07
Total aircraft drag	13.48	26.36	23.63

Table 5. Advanced technology baselines and goals

Discipline	Advanced technology	Baseline	Performance goal
Proprotor aerodynamics	Advanced proprotor	Cruise efficiency ~ 0.70	+0.07 effective rotor M_{DD}
Wing and airframe aerodynamics	Advanced leading and trailing edge devices	$C_{L_{max}}$ ~ 3.5 stall angle of attack = 22°	+0.5 $C_{L_{max}}$ +5° stall angle of attack
	Supercritical airfoil drag divergence	Early 80s supercritical airfoil performance	+0.05 in wing M_{DD}
	Low parasite drag	Typical turboprop transport aerodynamic efficiency (mean skin friction coefficient ~ 0.0042)	–10% parasite drag
Propulsion	Turboshaft engine sfc	GLC38-T1M1 turboshaft engine performance	–20% sfc
	Convertible engine sfc	GE38/CE4 convertible engine performance	–10% sfc
	Turboshaft engine power/weight	GLC38-T1M1 turboshaft engine performance	+40% power/weight
	Convertible engine power/weight	GE38/CE4 convertible engine performance	+17% power/weight
Structures/materials	Lightweight structural materials	Early 70s metal construction	–20% structural weight
	Lightweight drive system materials	Early 70s metal construction	–20% drive system weight

Table 6. Advanced aircraft results: optimization results

	Tiltrotor	Tiltwing	Folding tiltrotor
Gross weight, lb	29,441	29,438	36,337
Design variables			
Disk loading, lb/ft^2	21	21	14
Hover tip speed, ft/sec	742	750	750
Cruise tip speed, ft/sec	474	440	
Wing loading, psf	106.9	67.0	84.9
Wing thickness/chord	0.187	0.148	0.152
Wing chord/propeller diameter	0.235	0.244	0.209
Quarter chord sweep, deg	0.0	0.0	–20.2
Engine spanwise position ($2 * y_{eng}$/wing span)	1.0	0.814	1.0
Cruise altitude, ft	24,800	42,900	41,000

Table 7. Advanced aircraft results: vehicle performance

	Tiltrotor	Tiltwing	Folding tiltrotor
Gross weight, lb	29,441	29,438	36,337
Engine			
Sizing condition	Cruise	Cruise	Hover/cruise
Maximum power, hp	13,643	19,764	10,310
Transmission			
Sizing condition	Cruise	Cruise	Conversion
Maximum torque, ft-lb	62,969	43,834	62,741
Proprotor			
C_T/σ	0.125	0.125	0.125
Wing			
Sizing condition	Whirl flutter	Bending/whirl flutter	Bending
Cruise conditions			
Cruise L/D	7.78	12.48	11.42
Proprotor efficiency	0.77	0.77	N/A

Table 8. Advanced aircraft results: weight breakdown

Weight, lb	Tiltrotor	Tiltwing	Folding tiltrotor
Structural weight	5,551	7,338	7,160
Wing	1,192	2,363	1,698
Horizontal tail	232	265	303
Vertical tail	187	211	222
Fuselage	2,518	2,813	2,700
Landing gear	707	707	872
Nacelle	715	980	1,364
Propulsion weight	6,514	6,210	10,701
Proprotor system	1,977	1,253	4,119
Blade wt/proprotor	286		448
Hub wt/proprotor	703		925
Blade fold/proprotor	N/A		687
Drive system	2,544	2,462	2,538
Engine	1,419	1,944	3,238
Engine installation	199	272	453
Fuel system	375	278	352
Flight controls weight	2,393	1,784	3,705
Fixed equipment	4,800	4,800	4,800
Weight empty (WE/WG)	19,258 (0.65)	20,132 (0.68)	26,366 (0.73)
Fixed useful load	775	775	775
Payload	6,000	6,000	6,000
Fuel	3,409	2,531	3,197
Gross weight	29,441	29,438	36,337

Table 9. Advanced aircraft results: cruise drag breakdown

Equivalent flat-plate area, ft^2	Tiltrotor	Tiltwing	Folding tiltrotor
Wing	2.45	3.59	3.44
Fuselage	2.67	2.67	2.67
Horizontal tail	0.78	0.96	1.02
Vertical tail	0.65	0.65	0.65
Engine nacelle	1.79	2.10	1.61
Interference			
Wing-fuselage	0.36	0.16	0.22
Wing-nacelle	0.38	0.34	0.24
Folded blades	N/A	N/A	0.97
Miscellaneous	0.66	0.74	0.73
Total parasite drag	9.74	11.20	11.54
Induced drag	2.45	4.42	7.67
Compressibility drag	0.001	0.25	0.03
Total aircraft drag	12.19	15.87	19.24

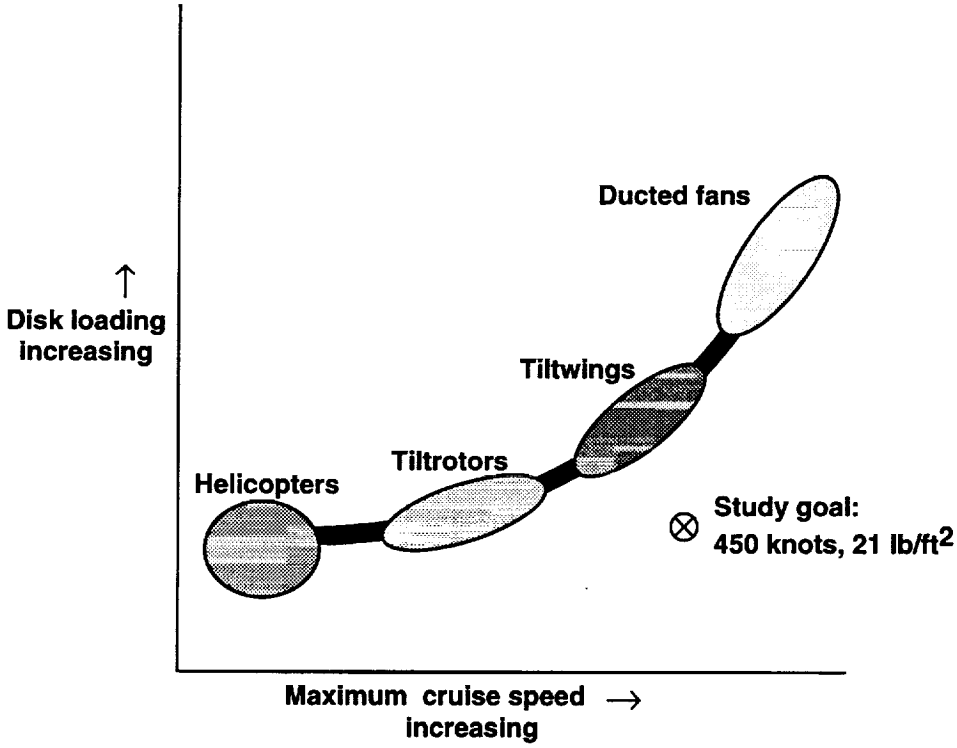

Figure 1. Historical disk loading vs. cruise speed trend.

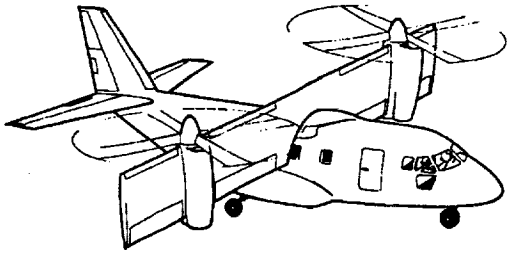

High-Speed Tiltwing (HSTW)

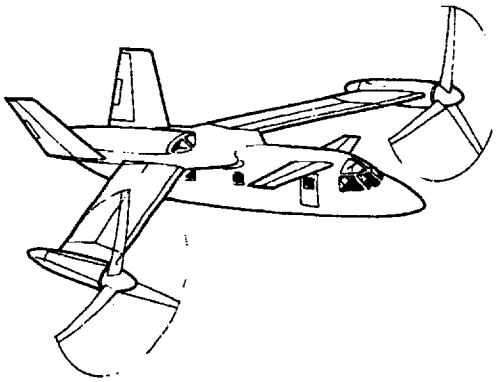

High-Speed Tiltrotor (HSTR)

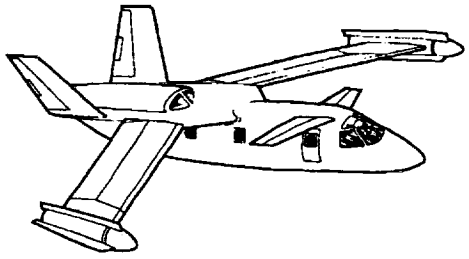

Folding Tiltrotor (FTR)

Figure 2. Study configurations.

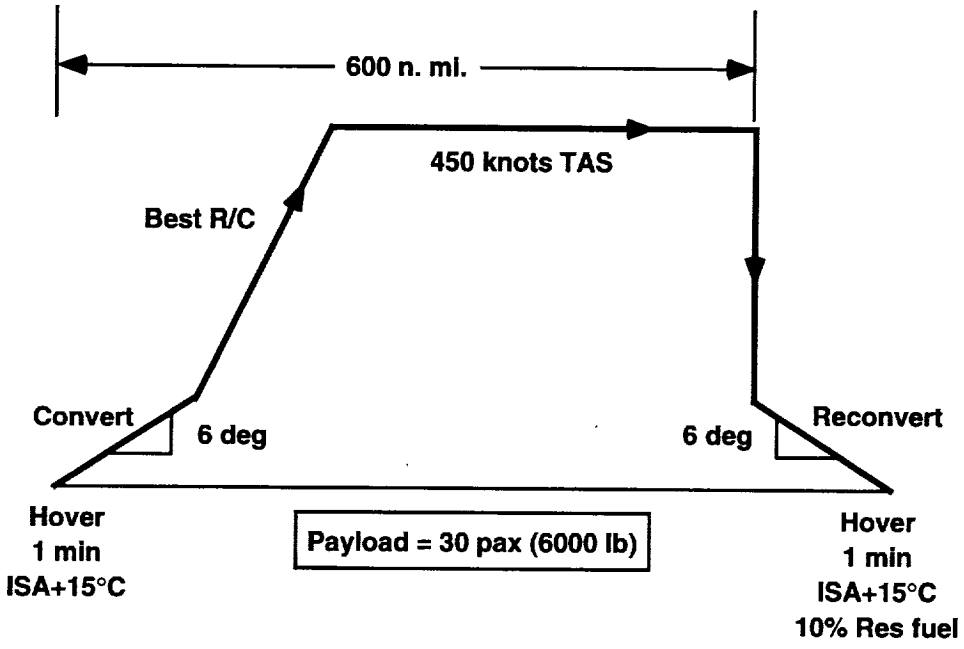

Figure 3. Civil transport mission.

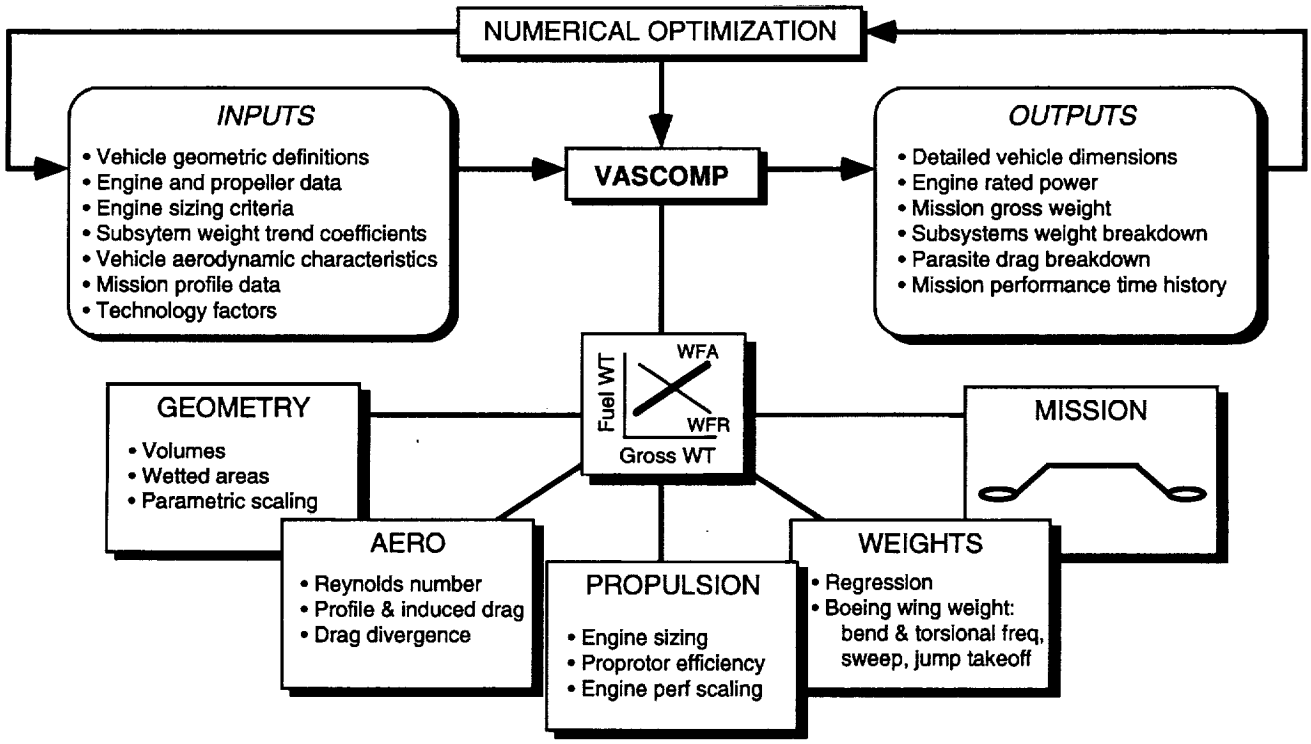

Figure 4. VASCOMP structure.

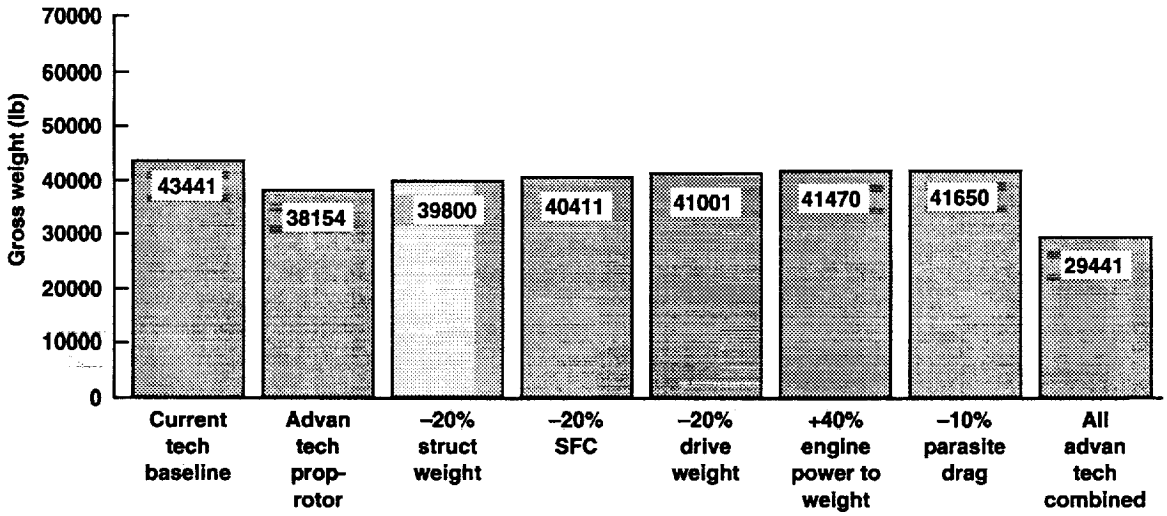

Figure 5. Tiltrotor advanced technology comparison.

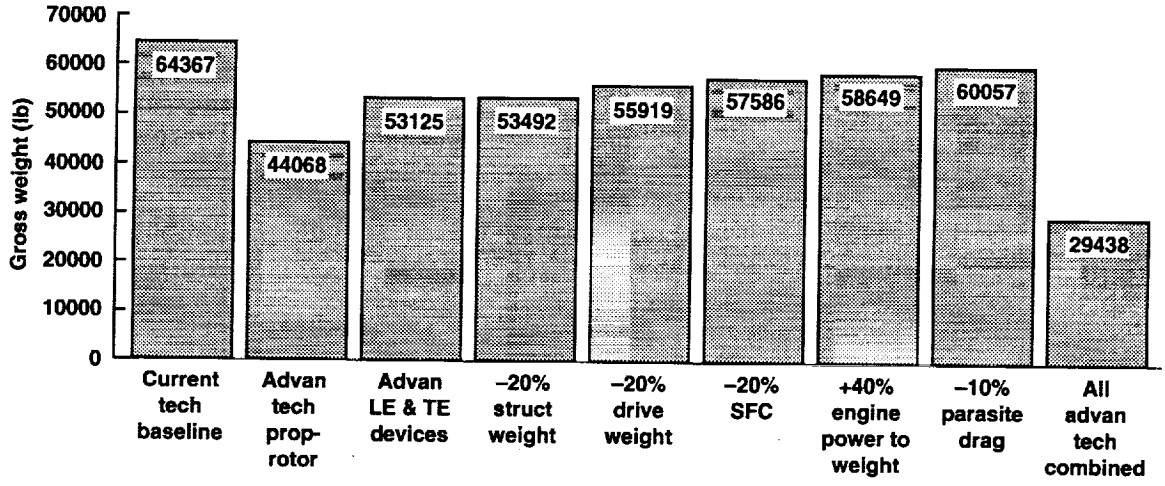

Figure 6. Tiltwing advanced technology comparison.

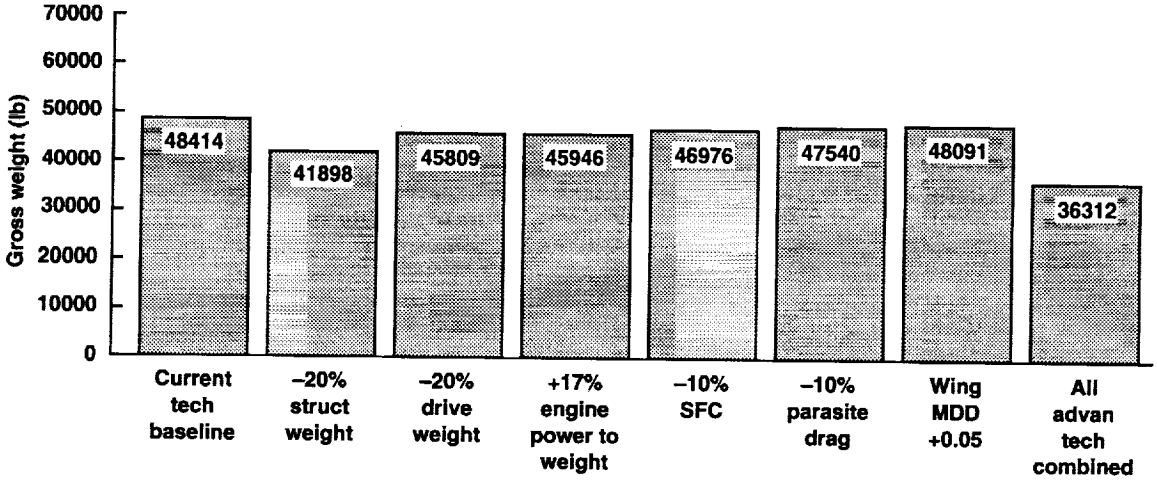

Figure 7. Folding tiltrotor advanced technology comparison.

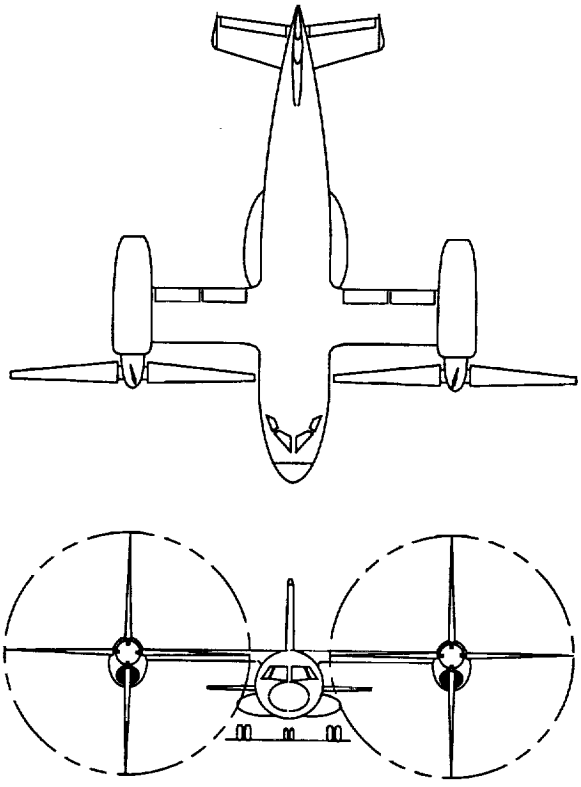

FUSELAGE:	Length, ft	59.3
	Width, ft	7.8
WING:	Area, ft^2	275.5
	Span, ft	39.2
	c/4 Sweep	0.0
	t/c	0.19
HORIZONTAL TAIL:	Area, ft^2	94.2
	Span, ft	19.4
	Moment Arm, ft	35.0
VERTICAL TAIL:	Area, ft^2	81.9
	Span, ft	12.8
	Moment Arm, ft	35.0
ENGINE NACELLE:	Length, ft	14.4
	Mean Diameter, ft	5.4
PROPROTOR:	Diameter, ft	29.9
	Solidity	0.135

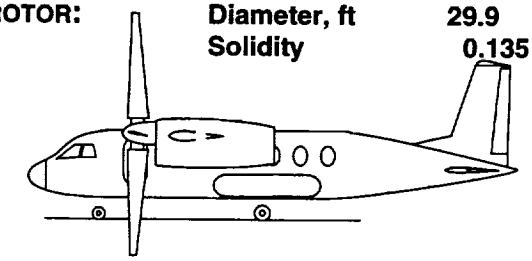

Figure 8. Advanced aircraft results. (a) Tiltrotor geometry.

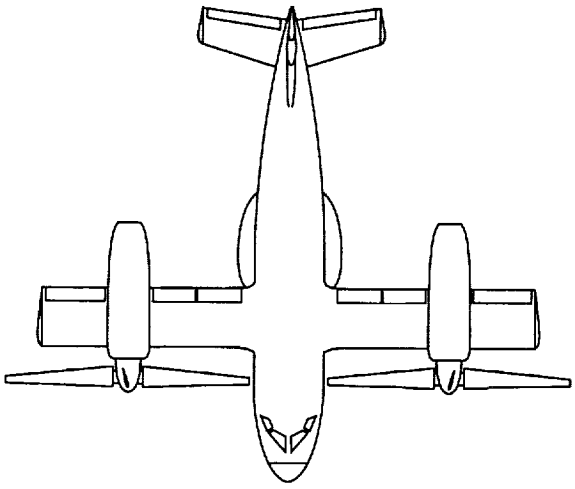

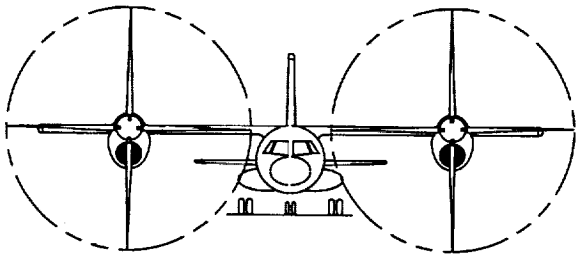

FUSELAGE:	**Length, ft**	**59.3**
	Width, ft	**7.8**
WING:	**Area, ft^2**	**439.5**
	Span, ft	**60.3**
	c/4 Sweep	**0.0**
	t/c	**0.15**
HORIZONTAL TAIL:	**Area, ft^2**	**117.6**
	Span, ft	**21.7**
	Moment Arm, ft	**35.0**
VERTICAL TAIL:	**Area, ft^2**	**81.9**
	Span, ft	**12.8**
	Moment Arm, ft	**35.0**
ENGINE NACELLE:	**Length, ft**	**16.8**
	Mean Diameter, ft	**5.9**
PROPROTOR:	**Diameter, ft**	**29.9**
	Solidity	**0.132**

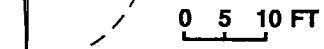

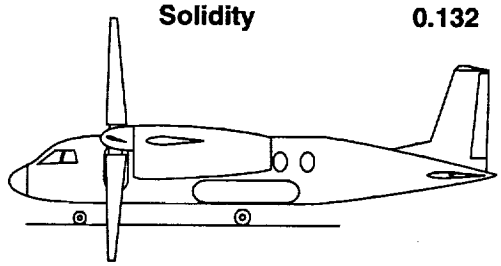

Figure 8. Continued. (b) Tiltwing geometry.

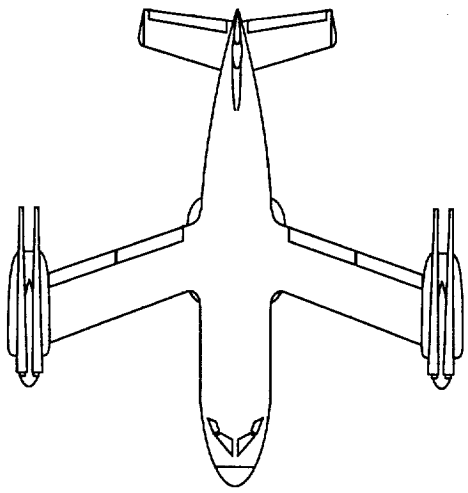

FUSELAGE:	Length, ft	59.3
	Width, ft	7.8
WING:	Area, ft^2	428.1
	Span, ft	50.2
	c/4 Sweep	-20.2
	t/c	0.15
HORIZONTAL TAIL:	Area, ft^2	125.8
	Span, ft	22.4
	Moment Arm, ft	35.0
VERTICAL TAIL:	Area, ft^2	81.9
	Span, ft	12.8
	Moment Arm, ft	35.0
ENGINE NACELLE:	Length, ft	12.9
	Mean Diameter, ft	5.0
PROPROTOR:	Diameter, ft	40.9
	Solidity	0.087

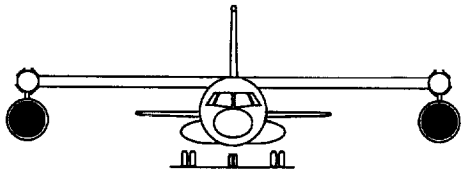

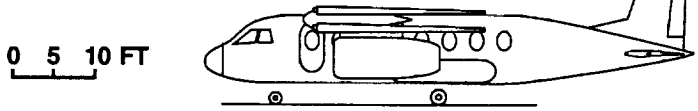

Figure 8. Concluded. (c) Folding tiltrotor geometry.

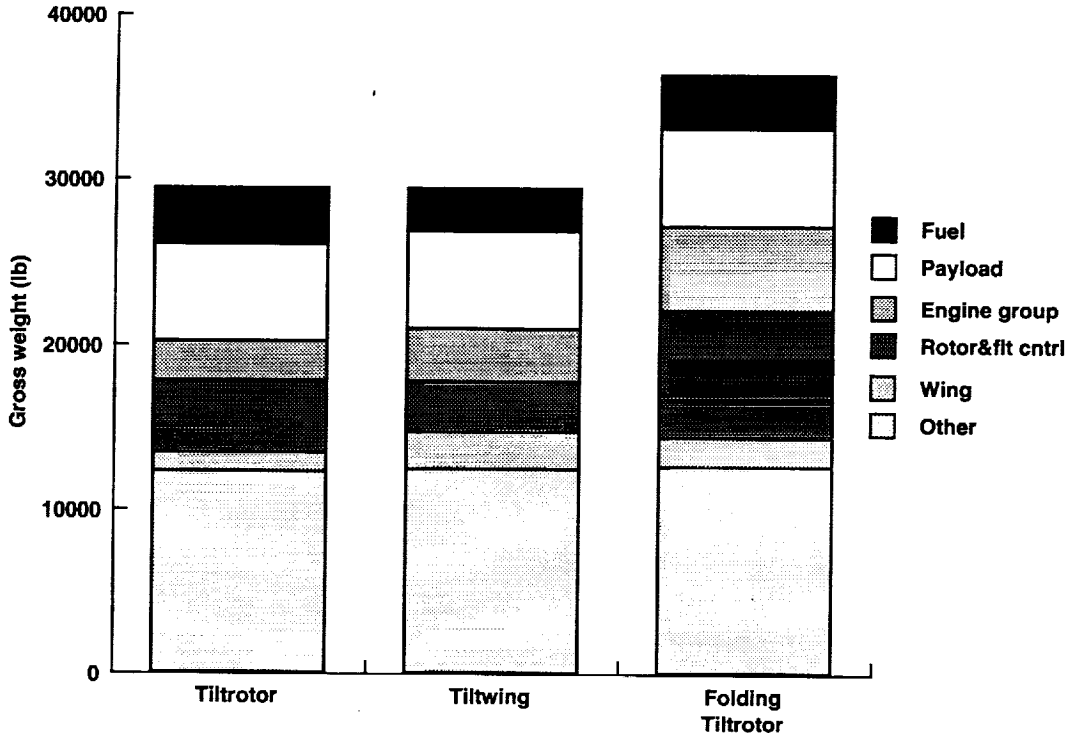

Figure 9. Advanced aircraft results: weights.

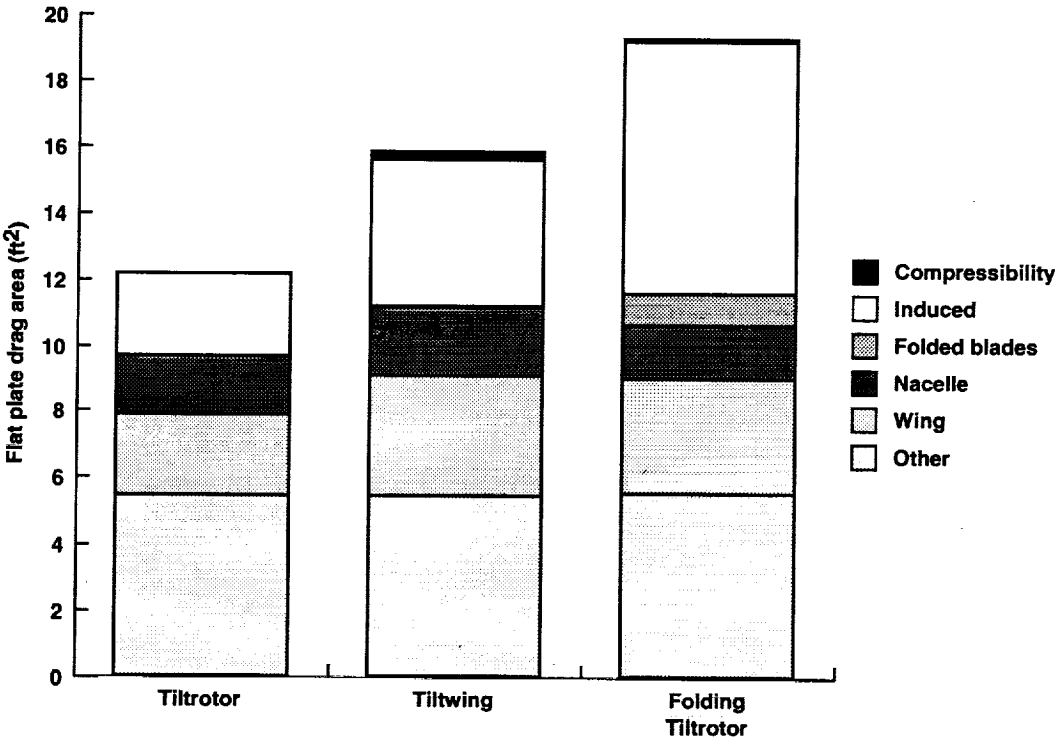

Figure 10. Advanced aircraft results: drag.

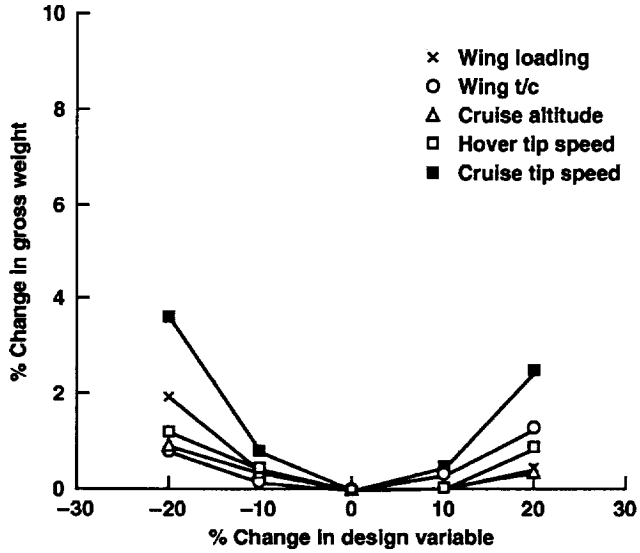

Figure 11. Tiltrotor design sensitivity.

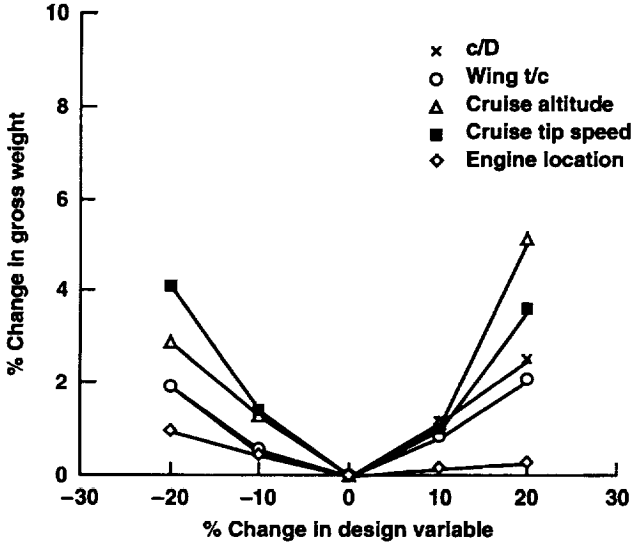

Figure 12. Tiltwing design sensitivity.

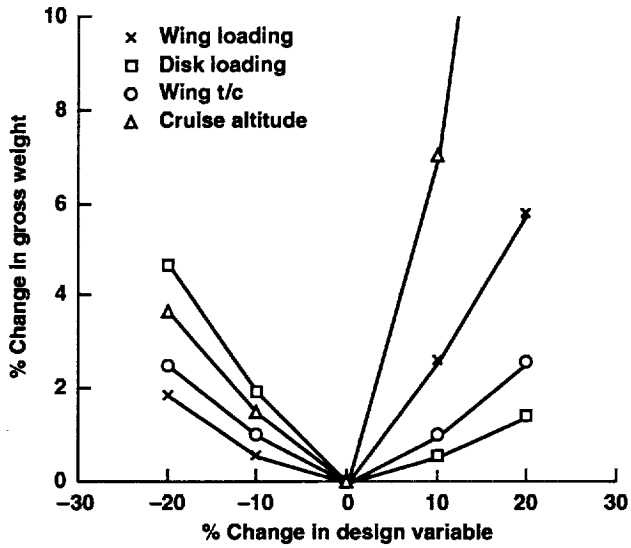

Figure 13. Folding tiltrotor design sensitivity.

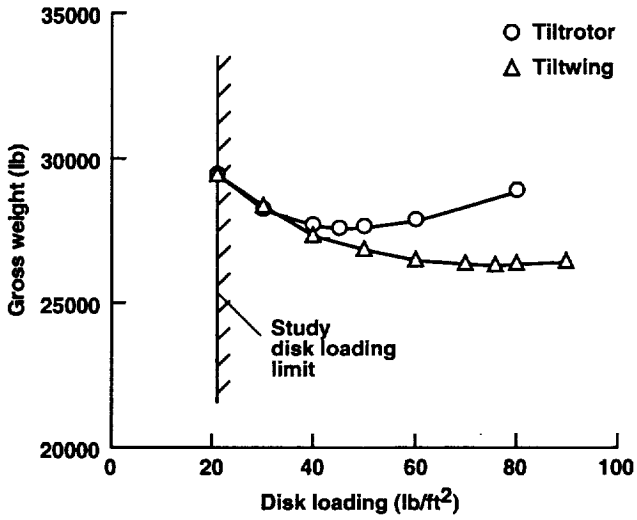

Figure 14. Gross weight trends with disk loading.

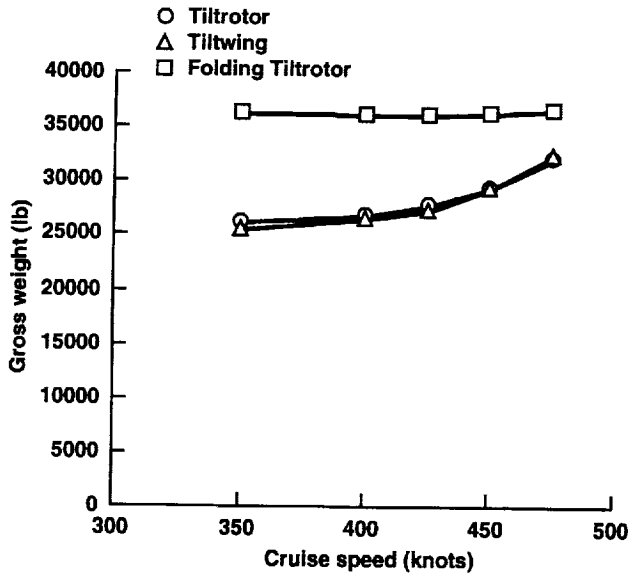

Figure 15. Gross weight trends with cruise speed.

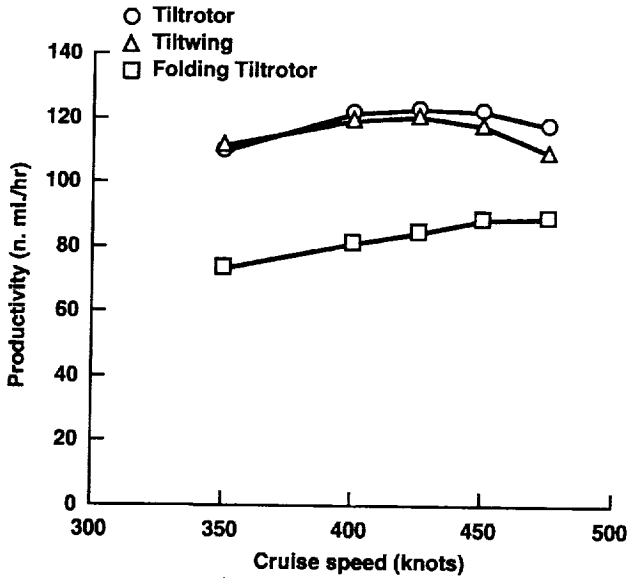

Figure 16. Productivity trends with cruise speed.

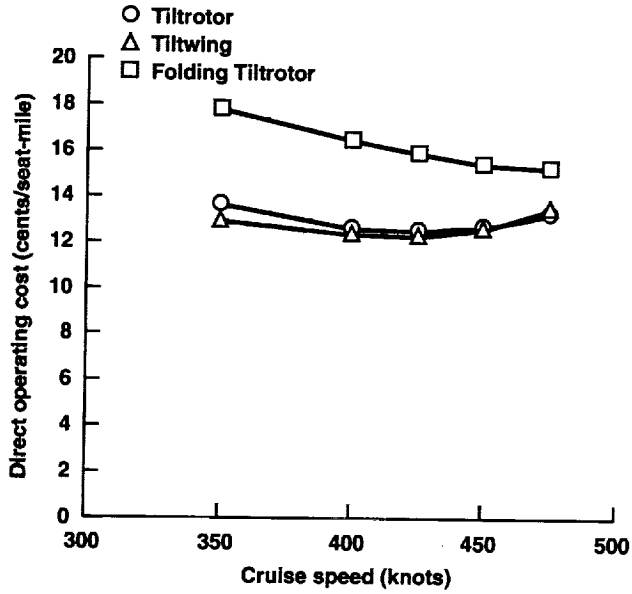

Figure 17. Direct operating cost trends with cruise speed.

REPORT DOCUMENTATION PAGE

Form Approved
OMB No. 0704-0188

Public reporting burden for this collection of information is estimated to average 1 hour per response, including the time for reviewing instructions, searching existing data sources, gathering and maintaining the data needed, and completing and reviewing the collection of information. Send comments regarding this burden estimate or any other aspect of this collection of information, including suggestions for reducing this burden, to Washington Headquarters Services, Directorate for information Operations and Reports, 1215 Jefferson Davis Highway, Suite 1204, Arlington, VA 22202-4302, and to the Office of Management and Budget, Paperwork Reduction Project (0704-0188), Washington, DC 20503.

1. AGENCY USE ONLY *(Leave blank)*	2. REPORT DATE	3. REPORT TYPE AND DATES COVERED
	April 1993	Technical Memorandum

4. TITLE AND SUBTITLE
Design Optimization of High-Speed Proprotor Aircraft

5. FUNDING NUMBERS
505-69-36

6. AUTHOR(S)
David R. Schleicher, James D. Phillips, and Kevin B. Carbajal

7. PERFORMING ORGANIZATION NAME(S) AND ADDRESS(ES)
Ames Research Center
Moffett Field, CA 94035-1000

8. PERFORMING ORGANIZATION REPORT NUMBER
A-93010

9. SPONSORING/MONITORING AGENCY NAME(S) AND ADDRESS(ES)
National Aeronautics and Space Administration
Washington, DC 20546-0001

10. SPONSORING/MONITORING AGENCY REPORT NUMBER
NASA TM-103988

11. SUPPLEMENTARY NOTES
Point of Contact: David R. Schleicher, Ames Research Center, MS 237-11, Moffett Field, CA 94035-1000
(415) 604-5789

12a. DISTRIBUTION/AVAILABILITY STATEMENT
Unclassified — Unlimited
Subject Category 05

12b. DISTRIBUTION CODE

13. ABSTRACT ***(Maximum 200 words)***

NASA's high-speed rotorcraft (HSRC) studies have the objective of investigating technology for vehicles that have both low downwash velocities and forward flight speed capability of up to 450 knots. This paper investigates a tiltrotor, a tiltwing, and a folding tiltrotor designed for a civil transport mission. Baseline aircraft models using current technology are developed for each configuration using a vertical/short takeoff and landing (V/STOL) aircraft design synthesis computer program to generate converged vehicle designs. Sensitivity studies and numerical optimization are used to illustrate each configuration's key design tradeoffs and constraints. Minimization of the gross takeoff weight is used as the optimization objective function. Several advanced technologies are chosen, and their relative impact on future configurational development is discussed. Finally, the impact of maximum cruise speed on vehicle figures of merit (gross weight, productivity, and direct operating cost) is analyzed.

The three most important conclusions from the study are (1) payload ratios for these aircraft will be commensurate with current fixed-wing commuter aircraft, (2) future tiltrotors and tiltwings will be significantly lighter, more productive, and cheaper than competing folding tiltrotors, and (3) the most promising technologies are an advanced-technology proprotor for both tiltrotor and tiltwing and advanced structural materials for the folding tiltrotor.

14. SUBJECT TERMS
Design optimization, High-speed rotorcraft, Tiltrotor, Tiltwing, Folding tiltrotor

15. NUMBER OF PAGES
40

16. PRICE CODE
A03

17. SECURITY CLASSIFICATION OF REPORT	18. SECURITY CLASSIFICATION OF THIS PAGE	19. SECURITY CLASSIFICATION OF ABSTRACT	20. LIMITATION OF ABSTRACT
Unclassified	Unclassified		